A comparison of different orthogonal techniques for the investigation of the conformational stability of NIST mAb in liquid formulations

MADELEINE ANDERSSON | MASTER OF SCIENCE THESIS IN PHARMACEUTICAL TECHNOLOGY 2020
DEPARTMENT OF FOOD TECHNOLOGY, ENGINEERING AND NUTRITION | LUND UNIVERSITY

A comparison of different orthogonal techniques for the investigation of the conformational stability of NIST mAb in liquid formulations

30hp MSc Thesis in Pharmaceutical Technology

Author
Madeleine Andersson

Industrial supervisors
Helen Sjögren and Signe Ridderberg, Ferring Pharmaceuticals

Academic supervisor
Marie Wahlgren, Department of Food Technology

Examiner
Lars Nilsson, Department of Food Technology

Lund University
Spring Semester 2020

Acknowledgements

I would like to thank Helen Sjögren and Signe Ridderberg that were my supervisors at Ferring Pharmaceuticals and Marie Wahlgren that was my academic supervisor. Thank you for your patience and your support, this would not have been possible without your help.

Furthermore, I would like to thank my colleagues at Ferring Pharmaceuticals and at the Department of Food Technology for being so helpful and friendly.

I would also like to show my appreciation to Ferring, the Department of Food Technology and to Solve for letting me use their labs and equipment. Furthermore, I appreciate the help I received from Applied Photophysics during the CD evaluation.

Lastly, I would like to thank family and friends for standing by me throughout my journey.

Abbreviations and symbols

Abbreviations and Symbols	**Definition**
A	amplitude
Abs	absorbance
B	baseline
C	concentration
CD	circular dichroism
CH2	constant heavy chain 2
CH3	constant heavy chain 3
D	dextrorotary
d	diffusion coefficient
D_0	self-diffusivity
Da	dalton
DLS	dynamic light scattering
DSC	differential scanning calorimetry
EMA	European Medicines Agency
Fab	fragment antigen-binding
Fc	fragment crystallizable
FWHM	full width at half maximum height
G	correlation coefficient
HCl	hydrochloric acid
I	intensity
IgA	Immunoglobulin A
IgD	Immunoglobulin D
IgM	Immunoglobulin M
IgG	Immunoglobulin G
k	Boltzmann constant
KCl	kalium chloride
k_D	interaction parameter
λ	wavelength
L	laevorotary
l	length
LCPL	left-hand circularly polarized light
mAb	monoclonal antibody
mdeg	milli degrees

mg	milli gram
mL	milli litre
M	molar
mM	milli molar
MQW	milliQ water
NaCl	sodium chloride
NaOH	sodium hydroxide
NIST	National Institute of Standards and Technology
nm	nano meter
Osmol	Osmolarity or osmotic concentration
PdI	polydispersity index
%Pd	percentage polydispersity
pI	isoelectric point
q	scattering vector
R_θ	Rayleigh ratio
RCPL	right-hand circularly polarized light
R_H	hydrodynamic radius
rpm	rotations per minute
σ	standard deviation
SLS	static light scattering
τ	delay time
T	temperature
t	time
T_{agg}	aggregation temperature
T_m	unfolding temperature or melting temperature
Trp	Tryptophan
UV	ultra violet
uL	micro litre
Z_D	Z-average
θ	measurement angle

Abstract

A great challenge during early development of medicinal antibodies is to determine the stability of the candidates. This is required to be able to select the candidates with the greatest developability. The stability of the candidates can be estimated using different orthogonal techniques and the aim of this investigation was thus to use orthogonal techniques for the investigation of conformational changes and aggregation of mAbs. The secondary aim was to obtain information concerning the effect that formulation components has on the stability of NIST mAb and which techniques that detects which conformational changes. The stability will be estimated for NIST mAb in liquid formulations where the mAb concentration, buffer type, tonicity, pH and storage time is altered. Differential scanning calorimetry (DSC), dynamic and static light scattering (DLS & SLS), circular dichroism (CD) and intrinsic fluorescence are the methods used to estimate the stability in the different formulations.

During the investigations it was noted that the instruments detect different conformational changes as they investigate different parts of the mAb and they received different peak temperatures of the conformational changes. Most instruments detect conformational changes in the span of 54-78°C. The order of the instruments that detected the first conformational change, from the lowest to the highest, was: DLS, CD, intrinsic fluorescence and DSC.

Additionally, the effect of the addition of salt was investigated using the nanoDSC and the Zetasizer and it was noticed that it caused destabilization of the mAb in both cases. The effect of pH on the mAb was investigated using DSC, DLS, CD and fluorescence. The CD measurements shows a positive linear trend between stability and pH for the investigated solutions, and a slight wavelength shift was detected during the fluorescence measurements between pH 5.2 and 5.7. Yet, the trend was not as clear for the DSC and it was unclear if DLS could detect a stability change based on the received results. Lastly, there are no clear correlations between the buffer types and the mAb stability for any of the investigated methods. Thus, it can be concluded that the methods detect different formulation changes, yet it is difficult to determine which investigational method is the most applicable in early formulation development.

Sammanfattning

Stabilitetsbestämning av läkemedelskandidater kan vara en utmaning under de tidiga stadierna av ett läkemeldels utveckling och det krävs att man väljer kandidaten med störst ”developability” möjlighet för att kunna skapa ett framgångsrikt läkemedel. Stabiliteten kan uppskattas med hjälp av olika ortogonala tekniker och därmed var det primära målet med denna rapport att använda ortogonala tekniker för att undersöka konformationsförändringar och aggregering hos antikroppar. Det sekundära målet var att få informatin om hur excipienter i en vätskeformulering påverkar stabiliteten av NIST mAb och vilka tekniker som upptäcker vilka konformationsförändringar. Detta kommer att undersökas med hjälp av differentiell svepkalorimetri (DSC), dynamisk och statisk ljusspridning (DLS & SLS), cirkulär dikroism (CD) och fluoresence, och de förutsättningar som kommer att ändras under undersökningarna är NIST mAb koncentrationen, buffer typen, toniciteten, pH och lagringstiden.

Undersökningarna visade att instrumenten upptäcker olika konformationsförändringar, varav de flesta ligger i ett temperaturspann mellan 54-78°C. Det visade sig även att DLS upptäckte den tidigaste konformationsförändringen följt av CD, fluorescens och DSC.

Dessutom underöktes effekten av salt i en formulering med hjälp av DSC och DLS, och salt hade en destabiliserande effekt i båda fallen. Effekten av pH på antikroppen undersöktes med hjälp av DSC, DLS, CD och fluorescens. Det fanns en positiv trend mellan stabilitet och pH i CD mätningarna, och det skedde ett litet våglängdsskifte i fluorescensmätningarna mellan pH 5.2 och pH 5.7. Emellertid fans det inte en lika tydlig trend I DSC mätningarna och det var oklart om DLS mätningarna kunde särskilja en stabilitetsförändring baserat på mätresultaten för NIST mAb vid olika pH. Slutligen uppmättes inga tydliga korrelationer mellan stabilitet och buffertyp i formuleringen, och därmed kan man dra slutsatsen att de olika instrumenten upptäcker olika formuleringsförändringar men att det är svårt att avgöra vilken metod som har störst appliceringsmöjlighet under de tidiga stadierna av formuleringsutveckling.

Populärvetenskaplig sammanfattning

En jämförelse av olika ortogonala tekniker för undersökningen av den strukturella stabiliteten av NIST mAb i vätskeformuleringar

Antikroppar har ett brett användningsområde med stor potential men det är svårt att skapa stabila lösningar. Den strukturella stabiliteten är en viktig faktor när man väljer läkemedels-kandidater, och i de tidiga utvecklings-stadierna görs predektiva undersökningar för att ta reda på varje kandidats stabilitet och utvecklings-potential. Därmed är det av största intresse att utvärdera hur antikroppars stabilitet påverkas av olika vätskeformuleringar och hur de predektiva undersökningar utvärderar stabiliteten.

Användandet av antikroppar i läkemedels-behandlingar har öppnat upp fantastiska möjligheter för att bota en bred variation av sjukdomar som antingen ej tidigare kunnat behandlats eller där de tidigare behandlingarna haft kraftiga biverkningar. Därmed har antikroppar en ljus framtid på läkemedels-marknaden och antalet godkända antikroppar har ökat stadigt under de senaste årtiondena. Det finns emellertid vissa svårigheter när det kommer till läkemedels-utvecklingen av antikroppar och ett stort hinder är antikropparnas stabilitet. En stabil antikropp krävs för att man ska kunna tillverka och transportera medicinen till patienten och det finns olika lösningar för att öka stabiliteten. Man kan till exempel tillsätta olika stabilisatorer till vätskelösningen som innehåller antikroppen, men innan man undersöker vilka stabilisatorer som passar den valda antikroppen så måste man bestämma vilken kandidat som har störst utvecklings-potential. Detta görs i ett tidigt stadie då man endast har en begränsad mängd av de olika kandidaterna och därmed görs predektiva undersökningar för att ta reda på varje kandidats stabilitet och utvecklingspotential.

En antikropps stabilitet kan delas upp i två huvudgrupper, nämligen den fysiska och den kemiska stabiliteten, och denna text har fokuserat på en antikropps aggregations-känslighet i olika vätskelösningar. Det tillhör den fysiska stabiliteten och innebär att man undersöker hur lätt antikropparna i lösningen klumpar ihop sig med varandra och därmed ändrar form och möjligtvis tappar sin medicinska funktion. En schematisk bild av en antikropp kan ses i Figur 1 nedan och från den kan man se att den består av två lätta och två tunga kedjor. Man kan även se att antikroppen delas upp i två regioner, en som heter Fab och en som heter Fc. Fab regionen är den region som binder sig fast till patogenen eller smittämnet och Fc regionen binder till andra immunceller som tar hand om smittämnet.

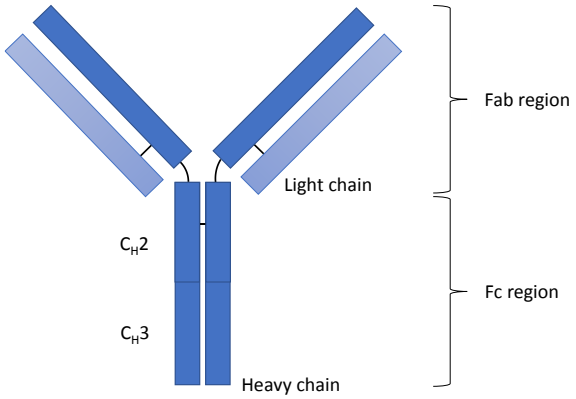

Figur 1. En schematisk representation av en antikropp där Fab och Fc regionerna är synliga. De tunga kedjorna är mörkblå och de lätta kedjorna är ljusblå. Fc regionen består av en C_H2 och en C_H3 region.

En metod som heter differentiell svepkalorimetri (DSC) användes för att undersöka vid vilken temperatur Fab och Fc regionen ändrade form och det visade sig att antikroppar i en vätskelösning med bordssalt ändrade form vid än lägre temperatur än en lösning utan salt. Detta visar att salt i detta fall hade en negativ inverkan på antikroppens stabilitet. Lösningar med två olika typer av buffrar och tre olika pH-värden undersöktes även, men en lika tydlig trend som med saltet kunde inte ses. Det resonerades därmed att

man möjligtvis kunde ändra dessa två förhållande beroende vilken region som var mest känslig för den valda antikroppen.

En annan metod som heter dynamisk ljusspridning (DLS) användes för att undersöka vid vilken temperatur antikropparna började klumpa ihop sig i lösningen, och även här återfanns samma stabilitetstrend mellan salthalt och stabilitet som i DSCn. Emellertid återficks inga tydliga och entydiga svar mellan stabiliteten och lösningens pH, buffer eller förvaringstiden i kylskåp. En möjlig orsak till de tvetydiga resultaten kan bero på att metoden är aggregationskänslig och att mätcellen troligtvis blev smutsig under undersökningarna vilket skulle ha en inverkan på mätresultaten.

Cirkulär dikroism (CD) är en tredje metod som användes för att komplementera undersökningsmetoderna och den kan mäta vilken 3D-struktur antikroppen har vid olika temperaturer. Dessa mätningar visade att antikroppen ändrade struktur vid en högre temperatur då lösningen hade ett högre pH. Dessutom tydde resultaten på att lösningens pH hade en inverkan på vilka delar av antikroppen som ändrade form.

De två sista metoderna som undersöktes var statisk ljusspridning (SLS) och fluorescence. SLS liknar DLS och mäter också partikelstorleken men på ett lite annorlunda sätt. Emellertid kunde man inte se någon aggregation under de mätningarna, vilket möjligtvis kunde bero på att koncentrationen var för låg för att detektorn skulle kunna mäta det. Fluorescence mäter ljusmängden som emitteras från fluorescerande delar av antikroppen och i detta fall undersöktes ljuset som emitterades från tryptofan, som är en aminosyra. Detta kan ge information om strukturförändringar och undersökningsresultaten tydde på att det skedde en strukturell föränding vid 64°C.

Sammanfattningsvis, konstaterades det att metoderna som undersöktes kan användas för att bestämma en antikropps stabilitet i olika vätske-formuleringar, och att de struktur-förändingarna som uppmättes skedde efter ca 58°C. Dessutom bekräftades det att salt har en negativ inverkan på korttidsstabiliteten av en antikropp och att korrelationen mellan en antikropps stabilitet och lösningens pH eller buffer är mer komplex. Slutligen kan man säga att läkemedelsindustrin har löst många av de stabilitetsutmaningar som proteinläkemedel har frambringat, och att antikroppar kommer vara den läkemedelstypen som leder oss in i en ny medicinsk era.

Contents

1. Introduction and Aim

The medicinal use of monoclonal antibodies (mAbs) is a large field of the parentally administered pharmaceuticals and approximately 20 parental formulations of mAbs per year has been approved by the European Medicines Agency (EMA) since 2013. (Gervasi, et al., 2017) A great challenge that occurs to many pharmaceutical developers is the task to select the monoclonal antibody that is going to be the active ingredient and to create a stable end-product that is patient compliant. An initial step, in addition to testing the mAb's binding affinity to the molecular target and other key aspects related to the biological activity, is to test the physical and chemical stability of all the newly discovered monoclonal antibodies with the desired properties in different media. This will support the selection of a suitable drug formulation which can be used in the non-clinical and early clinical trials. At such early stages of production only a limited amount of each mAb is available meaning that predictive methods that only use a small amount of mAb is required.

This thesis will focus on the physical stability of a generic monoclonal antibody in a liquid formulation. Aggregation is the main stability indicating parameter that this report will focus on and it can be used as a measure of a mAb's developability. Developability refers to the mAb's physiochemical properties that affect its suitability concerning manufacture, formulation and delivery (Temel, et al., 2016). The stability of the mAb will be investigated using differential scanning calorimetry (DSC), static and dynamic light scattering (SLS and DLS), circular dichroism (CD) and intrinsic fluorescence whilst altering the pH, tonicity and buffer type in the formulation. Formulations with compositions that are expected to differ in stability will be used to investigate how the results from the beforementioned techniques changes dependent on the formulation. Thus, the aim of the investigation is to use orthogonal techniques for the investigation of conformational changes and aggregation of mAbs. The secondary aim is to obtain information concerning the effect that formulation components has on the stability of NIST mAb and which techniques that detects which conformational changes.

2. Theoretical background

2.1. The Monoclonal Antibody

The general structure of an antibody is a large Y-shaped protein with an approximate weight of 150 kDa, see figure 1. They are built up of two heavy chains and two light chains, which all are covalently bound by disulphide bonds. The general structure of antibodies can be subdivided into five classes: IgA, IgD, IgE, IgG and IgM, see figure 2. Their two main differences are the glycosylation and position of their disulphide bonds; the last enabling some mAbs to form dimers (IgA) and pentamers (IgM), and others to have a flexible hinge region (IgA, IgD and IgG). The two fragment antigen-binding (Fab) regions consist of the section containing both the light chains and parts of the heavy chains, which forms the upper part of the Y. It is highly variable and binds to specific targets which induces the antagonistic effect. (Maverakis, et al., 2014) The fragment crystallizable (Fc) region consist of parts of the two heavy-chain domains (C_H2 and C_H3) and the hinge, if the mAb class has one. This forms the lower part of the Y and it enables binding with Fc receptors on immune cells (Temel, et al., 2016). The C_H2, Fab and C_H3 regions can unfold independently of one another in a noncooperative manner giving rise to multiple intermediate states between the native and the denatured protein. A denatured mAb has a changed tertiary and or secondary structure and has lost some or all potency. Denaturation of mAbs is in theory reversible if the conditions are changed back to favor the folded, native protein (Brange, 2000). However, in practice the process is considered irreversible as the reversing conditions often are too difficult to obtain. (Brange, 2000) (Temel, et al., 2016)

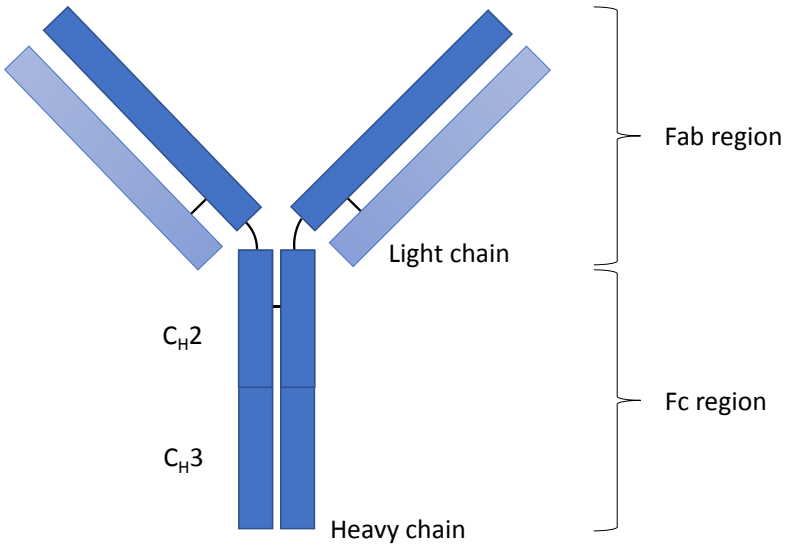

Figure 1. A schematic figure of a mAb where the Fab region and the Fc region is visible. The heavy chain is dark blue, and the light chain is light blue. The black lines between the chains are disulfide bridges. The Fc region of the heavy chain consists of the C_H2 and the C_H3 region.

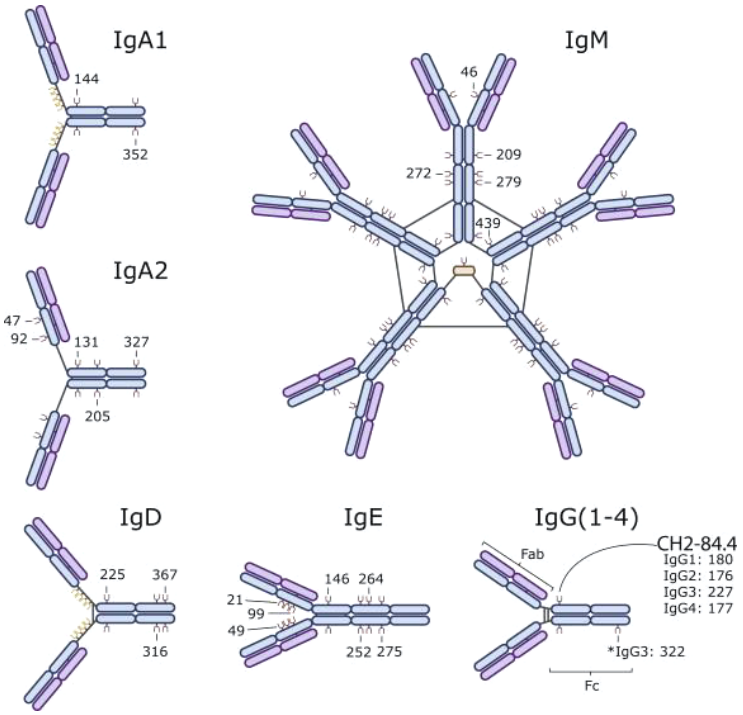

Figure 2. "Immunoglobulin Isotypes and their sites of glycosylation. Depicted here are the antibody structures including their sites of glycosylation (…). Each immunoglobulin is comprised of two heavy chains (blue) and two light chains (purple) that are linked together by disulfide bonds (black lines). IgA, IgD, and IgG have a flexible hinge region that link the Igs' antigen-binding Fab region to their Fc receptor-binding region. O-glycosylation sites are depicted in yellow and N-glycosylation sites are depicted in brown." (Maverakis, et al., 2014)

2.2 Monoclonal antibodies and their physical stability

The stability of a mAb can be divided into two main parts: chemical and physical stability, which are closely intertwined. Chemical stability depends on how persistent the mAb is to chemical reactions such as deamidation, fragmentation, oxidation and reduction. Physical stability depends on how persistent the mAb is to conformational changes from its native structure such as unfolding which can lead to aggregation and denaturation. When a mAb goes through a conformational change then one or more regions that are sensitive to chemical degradation can be exposed. This can in turn trigger a chemical reaction that alters the chemical composition of the mAb. The opposite is also likely to occur, where a chemical reaction triggers a conformational change. This is the reason why the two stabilities are so closely intertwined. (Le Basle, et al., 2019) The physical stability of mAbs is affected by protein-protein, protein-excipient and protein-solution interactions (Raznikov, et al., 2015).

2.2.1 Protein – protein stability, at different pH and concentrations

Proteins have side chains that are charged, and the overall charge of the protein is zero at the isoelectric point (pI). The pI-value is dependent on the protein's side chains and their interactions, and mAbs may therefore have multiple isoelectric points. These theoretical pI-values can be calculated but they might differ from the experimental pI-values, as the actual interactions in a complex formulation can be difficult to predict. (Gokarn, et al., 2015) Furthermore, when the pH approaches the mAb's pI its overall charge will decrease leading to less repulsion between the mAbs and more self-association. (Brange, 2000) It is therefore preferred to create a liquid formulation with a pH that is separate from any pI values.

In theory, positively and negatively charged regions could form in the tertiary structure if multiple charged side-chains are situated close to each other, which could result in a dipole moment. This could increase the protein's aggregation proneness and would then be an internal factor that affects stability. It would most likely be pH dependent.

Another cause for self-association is a high mAb concentration since the distance between the proteins will be smaller at higher concentrations which causes an increase in the interactions between the proteins. (Raznikov, et al., 2015)

2.2.2 Protein – solvent stability

Monoclonal antibodies have both hydrophobic and hydrophilic regions in their tertiary structure. The hydrophobic regions are mainly situated in the closely packed center of the mAb, where they are shielded from the polar solvent, and the hydrophilic regions are commonly situated at the surface. The solvents used must be compatible with injection into the human body and are therefore often water-based buffer systems. (Gervasi, et al., 2017) The monolayer of water molecules closest to the mAb can either have a hindered rotational freedom, which occurs if the molecules are strongly bound by two or more hydrogen bonds with the mAb, or a non-hindered rotational freedom. An increase in the rotation of the water molecules in the monolayer increase the flexibility of the mAb and thus also the total entropy and stability. Oppositely, the hydrophobic effect decrease entropy as the water molecules becomes ordered close to the hydrophobic regions of the mAb surface. (Brange, 2000) Hydrophobic regions at the surface of a protein are therefore more prone to aggregate as self-association of the hydrophobic surfaces would minimize the number of hydrophobic regions that are exposed to polar solvent. The use of a hydrophobic solvent would not be advised as it would result in the unfolding of the protein and a loss of activity.

2.2.3 Protein – excipient stability

Non-amino acid buffering agents

Buffers are commonly used in formulations to ensure a stable and optimal pH to increase mAb stability and solubility. Non-amino acid buffering agents are for example different weak acids such as sodium phosphate, sodium acetate, sodium citrate and TRIS (Gervasi, et al., 2017). These acids are the most commonly used non-amino acid buffering agents used in liquid drug formulations according to Gervasi et al in 2018. However, studies have been conducted where mAb self-buffering formulations have been investigated, and the results show that highly concentrated buffer free mAb formulations are a viable option to conventionally buffered formulations. (Bahrenburg, et al., 2015) (Gokarn, et al., 2008) Nevertheless, it is known that the buffer type influences the protein stability, as some proteins have a higher stability in one buffer compared to another. Yet, a reason to this stability difference is still to be found.

Tonicifiers

Tonicifiers are needed in injectables to create a solution that has the same tonicity as the human tissue that it is injected into, which is approximately 300mOsmol per liter (Drugs.com, 2020). Non-isotonic solutions that are injected into the body can cause pain and damage to the tissue. The two most commonly used ionic tonicifiers are sodium chloride (NaCl) and potassium chloride (KCl), but all excipients in a formulation except for water have a tonicifying effect. (Gervasi, et al., 2017) It is important to note that ionic components in the formulation may affect the stability of the protein as they can mask the repulsion between charged proteins leading to an increase in self-association. This is also commonly called the shielding effect. (Brange, 2000)

2.2.4 Triggers for conformational changes

Temperature

The movement and rotational ability of side-chains within the protein increase with increased temperatures. This results in a faster alteration of conformational change and a greater amount of energy available for those conformational changes, which enables less stable intermediate. At such an intermediate state the protein may either refold into its native state or unfold into a conformation that is closer to a denatured state. Hence, there is an increased risk of unfolding and denaturation at elevated temperatures.

Interfaces

Monoclonal antibodies can adsorb to both hydrophilic and hydrophobic surfaces such as for example glass and air respectively. Yet, the adsorption is generally greater at hydrophobic surfaces. (Brange, 2000) This can be explained by the increase in interactions between the hydrophobic inner of the protein and the hydrophobic surface, whilst still maintaining the hydrophilic interactions between the polar solvent and the hydrophilic parts of the protein. This results in a greater increase in entropy compared to protein absorption to a hydrophilic surface in the polar solvent. The adsorption rate is diffusion dependent on and affected by both protein concentration and temperature (Brange, 2000). The amount of protein molecules adsorbed usually increase steeply with time until the surface is saturated. If the amount of adsorbed mAb is plotted against time it will look like a plateau is reached after a certain amount of time in a graph over ideal adsorption. However, sometimes the well-defined plateau is not reached, and the amount of adsorbed proteins continues to increase but with a decreased adsorption rate. This could be due to aggregation of the proteins on the surface. (Brange, 2000)

Aggregation is generally greater when the proteins are adsorbed at a surface as the proteins are situated closer together than they would be in the solution. Furthermore, the protein can change conformation and expose hydrophobic regions in contact with the surface resulting in more aggregation, largely due to the hydrophobic effect. This is a great problem if the storage vessel has a large area of hydrophobic surfaces or if there is a liquid-air interface that the protein can adsorb to. The risk of adsorption to the liquid-air interphase is especially large during agitation as new interphase area without adsorbed protein is exposed. (Brange, 2000)

2.3 Key techniques

The following orthogonal techniques are used in the experiments and will be further discussed below: differential and static light scattering (DLS and SLS), differential scanning calorimetry (DSC), circular dichroism spectroscopy (CD) and intrinsic fluorescence.

2.3.1 DSC

During a DSC scan a sample cell and a reference cell is heated to maintain the same temperature during each heating cycle. Yet, the unfolding of a mAb is endothermic meaning that the sample cell will require more energy to maintain the same temperature as the reference cell. (Temel, et al., 2016) This information can be recalculated into the specific heat capacity of the mAb and plotted if the amount of mAb in the sample is known. Deconvolution of the received curve typically result in three different peaks representing the C_H2, Fab and C_H3 regions of the mAb, see Figure 3. The unfolding temperatures,

enthalpy change, and activation energy, which is the peak height, for each region can then be seen in the plot. The unfolding temperature, T_m, is given by the peak position, the enthalpy correspond to the area under the peak and the activation energy is represented by the sharpness and skewedness of the peak. (Freire, 2019) High T_m values and high activation energies are indications of a better long-term low temperature stability according to Freire (2019) and the Fab region generally has the highest enthalpy transition according to Temel et al. (2016). Furthermore, Temel et al. (2016) states that the Fab region gives a better indication of the stability than the other regions.

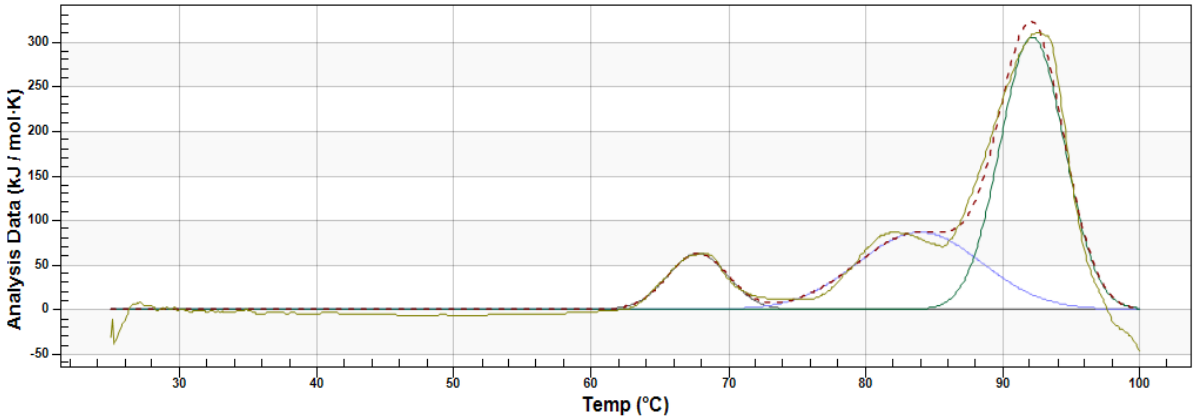

Figure 3. The energy required for the unfolding of NIST mAb in a liquid formulation is represented by the light green solid line, which has three unfolding peaks. The deconvolution is the fitting of three separate normal distributions to the received data. The red dotted line is the resulting curve of the deconvolution.

The denaturation rate can be calculated using non-linear squares analysis for each peak, which estimates the kinetic parameters for each peak. This is possible when an irreversible aggregation is assumed and not when an equilibrium model is used. The denaturation rate at T_m for two different mAbs might be the same, yet the denaturation rate might decrease differently with temperature. A high activation energy generally means that it will have a faster rate decrease with a decrease in temperature, leading to better long-term low temperature stability. Note that the smaller peaks, usually arising from the C_H2 and C_H3 region, thereby will have a lower stability at low temperatures meaning that it is possible that they are the main cause of aggregation at low temperature storage, which is the opposite case of high temperature stability measurements. (Freire, 2019)

It is important to note that the folding-unfolding of the mAb in the DSC experiments isn't in an equilibrium, since the mAb cannot return to its native state in an easy manner after a run that exceeds the temperature of all transitions. This means that equilibrium models give incorrect and sometimes misleading information as they do not take the "*asymmetry towards the low temperature end*" of the irreversible unfolding into account according to Freire (2019). Furthermore, an equilibrium model which is based on thermodynamics cannot estimate the denaturation rate and activation energy. This is only possible using a kinetic model which is independent of the equilibrium assumption according to Freire. (Freire, 2019) Nevertheless, it can be discussed whether the commonly used method of obtaining the results during a slow temperature ramp, where an equilibrium between the native and the unfolded intermediate is created at each temperature point, is adequate for developability measurements. This method is commonly considered adequate if no irreversible aggregation or degradation occurs. (Temel, et al., 2016) Yet, it is known that significant irreversible aggregation commonly occurs at the temperatures above the first melting temperature in a DSC scan. Gokarn et al. (2015) showed that mAb has an almost complete conformational reversibility during temperature

ramping that only exceed the first NIST mAb peak but only a partial reversibility if the second and third transition temperatures are exceeded.

2.3.2 DLS

A dynamic light scattering (DLS) instrument measures the light scattering intensity of the sample. The light scatter intensity will look random over a long time-span but smooth and continuous over a short time span, which is due to the Brownian motion (diffusion) of the particles that scatter the light in the sample. Small particles diffuse faster than large particles and will thus give rise to a random signal more quickly than a large particle, as the particle first will scatter the light from one position and then move randomly to a new position in the solution. This information enables us to differentiate particles based on size and an aggregation temperature (T_{agg}). The T_{agg} can be estimated as the drastic size increase that occurs when a sample is heated. (Mattison & Nobbmann, 2011). The aggregation temperature is lower than the melting temperature (T_m) that is estimated through for example DSC or CD (Nobbmann, 2017). This is because T_m is the temperature where the mAb has transitioned into one of its transition states, which is separate from the native state. Thus, it is considered to be completely or close to completely denatured, which reasonably would occur at a temperature that is above the onset of aggregation. (Nobbmann, 2017)

The following six equations (I-VI) connects the particles' Brownian motions to different parameters that are used to evaluate the particle populations within a sample. The correlation coefficient, which is displayed over time in a correlogram, is a measure of the degree of non-randomness in a seemingly random scattering intensity signal. It is calculated through Equation I below, where G is the correlation coefficient, τ is the delay time and, t is the time, I is the intensity and the brackets (<>) indicates averaging over t. (Gervasi, et al., 2017)

$$G(\tau) = \frac{\langle I(t)I(t+\tau)\rangle}{\langle I(t)\rangle^2} \qquad \text{Equation I}$$

The diffusion coefficient (d) can be calculated from the correlation coefficient using Equation II which is a cumulants analysis. B is the baseline of the correlogram at infinite time, A is the amplitude at time zero, q is the known scattering vector and τ is the delay time. (Gokarn, et al., 2015)

$$G(\tau) = B + Ae^{-2q^2 d\tau} \qquad \text{Equation II}$$

The diffusion coefficient can then be used to calculate the hydrodynamic radius (R_H) of the particles in the sample, using Stokes-Einstein equation which is seen in Equation III (Gokarn, et al., 2015). The hydrodynamic radius is defined as the *"radius of a hard sphere that diffuses at the same rate as the protein. Includes hydration and shape effects"* according to Mattison & Nobbmann (2011). In Equation III k is the Boltzmann constant, T is the Temperature and η is the viscosity of the medium (Gokarn, et al., 2015). The calculated hydrodynamic radius based on the cumulants analysis is often called the Z-average size, which is based on the *"intensity weighed mean size of the distribution"* Mattison & Nobbmann (2011).

$$R_H = \frac{kT}{6\pi\eta d} \qquad \text{Equation III}$$

The diffusion coefficient correlates to the diffusion interaction parameter (k_D) through Equation IV, where D_0 is the self-diffusivity and C is the concentration (Gokarn, et al., 2015). The diffusion interaction parameter is proportional to the virial coefficient (B_{22}) and therefore representative of the protein's tendency to self-associate and aggregate. k_D is commonly plotted against concentration, which graphically depicts the aggregation tendency. A positive slope indicates repulsion between the proteins whereas a negative slope indicates attractions. (Mattison & Nobbmann, 2011)

$$d = D_0(1 + k_D C) \qquad \text{Equation IV}$$

The polydispersity index (PdI) and the percentage polydispersity (%Pd) of a sample indicates how wide the size distribution is within a sample population. A %Pd value of <15% is usually desirable as it indicates a monodisperse sample. The relation between PdI, %Pd, Z-average (Z_D) and the distribution standard deviation (σ) is shown in Equation V and VI below. (Mattison & Nobbmann, 2011)

$$\%Pd = 100\sqrt{PdI} \qquad \text{Equation V}$$

$$PdI = \frac{\sigma^2}{Z_D^2} \qquad \text{Equation VI}$$

To optimally determine the size and the aggregation temperature, according to Mattison & Nobbmann (2011), then a smooth sigmoidal correlation curve with a correlation coefficient intercept above 0.8 is desired. A correlation coefficient intercept below 0.5 is not considered good and could be an indication of a too low sample concentration, a fluorescing sample, a too highly concentrated sample, a dirty cuvette or poor system alignment. Firstly, if the sample concentration is too low there will not be enough dispersed particles that scatter the light, resulting in the low correlation coefficient intercept. This can be improved by increasing the sample concentration. Secondly, a fluorescing sample will absorb light and send out light of a different wavelength causing noise and randomicity, leading to a lower correlation coefficient intercept. This can be improved by adding a light filter that removes any light of the fluorescing wavelength. Thirdly, a too high sample concentration can cause multiple scattering as the light scattered from one particle can be subsequently scattered again by another particle before reaching the detector. This can be improved by decreasing the sample concentration. Furthermore, diffusion can be restricted at higher concentrations due to crowding or exclusion effects, leading to a higher viscosity than that of the pure solvent. This will have a direct effect on the estimated size of the sample population, as size is inversely proportional to viscosity in the Stokes Einstein equation, see Equation III above. Restricted diffusion will lead to particles being estimated to a larger size than they are. This can be avoided by either lowering the sample concentration so that the viscosity of the sample is closer to the solvent viscosity, or by measuring and calculating the R_H using the sample viscosity instead of the solvent viscosity. Fourthly, a dirty cuvette can give rise to unexplainable peaks and an increased PdI. This can be avoided by finding a thorough cleaning program that removes any trace protein in the cuvette in between the sample measurements. Lastly, a poor system alignment can be a result of not using the optimal scattering volumes, scattering angles or laser wavelengths, which will affect the results and interpretations in a non-beneficial way. Larger particles can be recorded whilst using a large scattering volume but there will be a decrease in sensitivity, whereas a small scattering volume will have a smaller size range and a higher sensitivity. This will result in a difference of the intensity weighed Z-average value between the two systems if large particles are present. A classical 90° scattering angle generally has a smaller scattering volume and higher sensitivity

than a backscattering angle system. It might therefore be more suitable for solutions with a low concentration of small particles, whereas a backscattering angle system is more suitable for solutions with a higher concentration of larger particles as it has a larger scattering volume and is less affected by multiple scattering effects. Laser wavelength is most commonly altered because of a fluorescing or absorption problem with the sample, but it can also be altered to increase sensitivity as it is proportional to the inverse of the wavelength raised to four, λ^{-4}. (Mattison & Nobbmann, 2011)

It is important to note that DLS is extremely sensitive to large aggregates due to the R^6 dependence between the intensity weighed distribution and the volume or mass weighed distribution. The dependence is explained using Mie theory and means that the scattering intensity from an aggregate will be much larger than from a monomer. It is therefore good to remember that the plotted intensity of two separate population will show a much larger scattering intensity peak for the large population than the small, even though the sample contains the same number of particles in each population. This leads to a relatively low resolution between sample populations and results in the difficulty in resolving monomer peaks from dimer peaks. A three-fold size difference is required to have a baseline resolution between the populations. (Mattison & Nobbmann, 2011) It is also important to note that a dataset can have multiple solutions during analysis and that different algorithms thus might give different results (Malvern, 2020). For example, the analytical algorithm in the Zetasizer has a PdI-value that is "*more representative of a protein*", whereas the general algorithm *"suits most samples"* according to Malvern (2020).

2.3.3 SLS

A static light scattering (SLS) instrument measures the light scattering intensity of the sample similarly to a DLS instrument, yet oppositely it measures the intensity height instead of the intensity difference over time, see figure 4 below. Through this the size change of the particles in the solution can be estimated. There are four different methods of measuring the SLS which have different benefits and drawbacks. One of the most common methods is to measure the right-angle light scattering (RALS). This gives the best signal to noise ratio, but it is unable to measure the radius of gyration (R_g) and the scattering is assumed to be isotropic. This means that the intensity of the scattered light is independent of the scattering angle, which is often not the case for larger molecules. One method of estimating the R_g and the molecular weight of the scattering molecules is to create a Guinnier plot, where KC/ R_θ is plotted against $\sin^2(\theta/2)$ see figure 5. K is a constant, C is the concentration, R_θ is the Rayleigh ratio and θ is the measurement angle. The molecular weight can be estimated using RALS but not the R_g as seen in figure 5. This is due to the fact that R_g is estimated using the initial slope created by measurements at multiple angles. (Malvern Instruments, 2015)

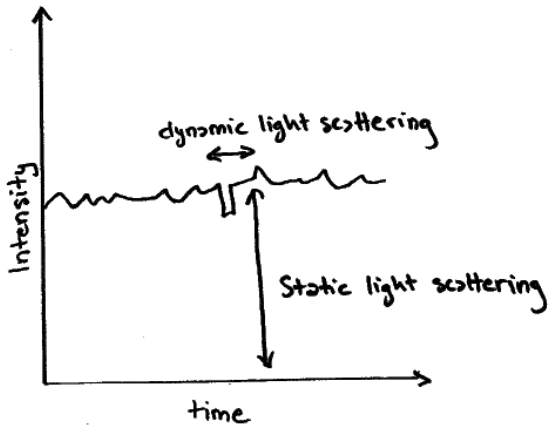

Figure 4. The DLS measures the intensity fluctuations over a short time period whereas the SLS measures the intensity at a certain time point.

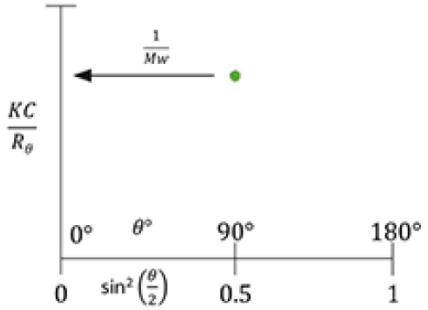

Figure 5. "When using RALS, the Debye plot is reduced to a single point which is assumed to be equal at every angle and therefore equal 1/Mw." (Malvern Instruments, 2015)

2.3.4 CD

Circular dichroism (CD) measures the difference in absorption of left-handed and right-handed circularly polarized light of chiral chromophores, see equation VII where Abs is the absorbance and λ is the wavelength. LCPL and RCPL stands for left-handed and right-handed circularly polarized light respectively and optically active chiral molecules commonly have an L or a D as a prefix, which stands for laevorotary and dextrorotary meaning left-handed and right-handed rotation in Latin respectively (Gokarn, et al., 2015) (Applied Photophysics, 2012) (Helmenstine, 2019). Absorption and ellipticity, θ, are closely related and can be interconverted through equation VIII below, from Applied Photophysics (2020). Ellipticity is often divided by a thousand and written as millidegrees or mdeg due to the small angle of many measurements. (Applied Photophysics, 2020)

$$\Delta Abs(\lambda) = \Delta Abs(\lambda)_{LCPL} - \Delta Abs(\lambda)_{RCPL} \qquad \text{Equation VII}$$

$$\Delta Abs = \frac{\theta}{32.932} \qquad \text{Equation VIII}$$

The secondary structure of a protein can be estimated while measuring the absorbance in the far-UV region, which spans from 180 to 250nm. This is due to the absorbance of the peptide linkages in the backbone (Applied Photophysics, 2019). Alpha helices have a maximum absorbance at 193nm and two minimum absorbances at 208 and 222nm. Beta sheets have a maximum absorbance at 195nm and a

minimum absorbance at 218. Random coils have a maximum absorbance at 215nm and a minimum absorbance at 195, see Figure 6. (Gokarn, et al., 2015) Far-UV measurements have a higher sensitivity than near-UV measurements as there are more peptide linkages than chromophores or disulphide bonds. Hence, a lower concentration or a smaller pathlength can commonly be used in far-UV measurements. Near-UV measurements can be used to evaluate changes in the tertiary structure of a protein, and the measurements span used is often 250 to 340nm. The near-UV spectra cannot be used in the same manner as the far-UV spectra where a protein's main secondary structure can be estimated. Instead it can be used to estimate specific structural changes that affect tryptophan, tyrosine, phenylalanine and disulphide bonds. (Chiralabs, 2020) This is because the disulphide bonds and the non-chiral side chains of aromatic amino acids are chromophores that are affected by their chiral environment (Applied Photophysics, 2019) (Chiralabs, 2020). Tryptophan give rise to ellipticity signals at 290-305nm, tyrosine at 275-282nm and phenylalanine at 255-270nm. The contribution from the disulphide bonds to the near-UV spectra ranges from approximately 250-330nm but it is often most visible between 310-330nm as this is outside the range of tryptophan, tyrosine and phenylalanine. To estimate the structural changes that occurs one can compare the magnitudes and finer features that exist in the spectra. If for example a magnitude loss occurs but the fine features remain then it is likely that the disulphide bonds have started to move and not the aromatic amino acid. However, if the fine features change then it is instead likely that the aromatic amino acid has started to move. If there are visible changes above 330nm then it can suggest that precipitation of the sample has occurred if there are no intrinsic chromophores that can explain the light absorption. (Chiralabs, 2020)

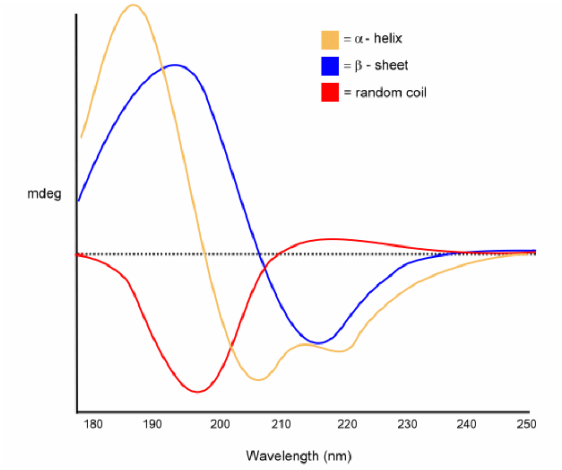

Figure 6. A schematic representation of the absorbance for alpha-helices, beta-sheets and random coils. Millidegrees is directly correlated to absorbance. (Pronalyse, 2020)

2.3.5 Intrinsic scanning fluorometry

Intrinsic fluorescence has the advantage of not using a probe that could interfere with the conformation of the mAb and instead measures the emission of light from a fluorescing species within a molecule when it is exposed to short wavelength light. The light emission ends when the excitations light is removed. (Aulton, 2007) Hence, fluorescence is measured at a 90° angle to the incident light.

There are three naturally fluorescing amino acids, namely tryptophan, tyrosine and phenylalanine. Their fluorescing properties are dependent on the absorptivity and the quantum yield of the amino acid. Phenylalanine has the lowest absorptivity and quantum yield of the three, see Table 1, and is therefore not the first-hand choice when measuring fluorescence. Tyrosine has the second highest absorptivity and quantum yield and it can be used for fluorescence measurements, yet its emission is

often quenched in native proteins. Hence, tryptophan is often the preferred fluorophore. Tryptophan (Trp) has an excitation wavelength of 280nm and an emission wavelength of 348nm, yet it is highly sensitive to its local environment causing a red shift in polar environments and a blue shift in non-polar environments. A very blue shifted emission wavelengths of Trp can be seen in the protein azurin which has an emission wavelength of 308nm. Oppositely, the Trp that exist in denatured glucagon is very red shifted and has an emission wavelength of 352nm. (Ghisaidoobe & Chung, 2014) Hence, it is reasonable to measure a rather wide emission wavelength span when investigating how the configuration changes in proteins.

Table 1. Fluorescence properties of aromatic amino acids in water at neutral pH. (Ghisaidoobe & Chung, 2014)

	Absorption		Fluorescence	
	λ(nm)	Absorptivity (ϵ)	λ(nm)	Quantum Yield (Φ_F)
Tryptophan	280	56000	348	0.2
Tyrosine	274	1400	303	0.14
Phenyl alanine	257	200	282	0.04

3. Materials and method

Table 2 displays the chemical formula, the CAS number and Supplier of all the chemicals that are used during the experiments.

Table 2. The chemicals used during all the experiments are listed below.

Name	Chemical formula	CAS and ID number	Supplier
NIST mAb	N/A	NIST8671	Sigma Aldrich
L-histidine	$C_6H_9N_3O_2$	71-00-1	Sigma Aldrich
MQW	H_2O	7732-18-5	N/A
Citric acid monohydrate	$C_6H_8O_7$ H_2O	5949-29-1	VWR
Sodium hydroxide	NaOH	1310-73-2	VWR
Hydrochloric acid	HCl	7647-01-0	VWR
Sodium chloride	NaCl	7647-14-5	Th. Geyer

The NIST mAb from Sigma-Aldrich is an IgG1 humanized monoclonal antibody with a molecular mass of approximately 150 kDa. One vial contains 800 µL of 10 mg/mL NIST mAb in a 25mM L-Histidine buffer at pH 6.0. (Aldrich, 2020)

3.1 Methods

3.1.1 NanoDSC

A temperature ramp of 1°C per min was conducted between 20-100°C using the NanoDSC and corresponding autosampler from TA Instruments. The instrument required 500uL sample volume and 800uL of the reference liquid. All liquids that were inserted into the wells in both the reference tray and the sample tray were degassed using the degassing station from TA Instruments. The results were analyzed using the software NanoAnalyze.

3.1.2 DLS

A temperature ramp of 1°C per min was conducted between 20-90°C using a Zetasizer APS from Malvern. CORNING assay plates with a flat bottom, non-binding surface, polystyrene (96 and 384 wells) were used during the experiments. The 384 well plate required a minimum sample volume of 20uL. The plates were centrifuged to remove bubbles using a plate centrifuge and a liquid cooler from Melcor corporation was used to cool the plates during the runs. The datasets were analyzed using the general and analytical algorithm in the Zetasizer software and the calculated Z-average was then plotted against temperature.

A step-wise temperature increase of 10°C from 25°C until 60°C was conducted on the DynaPro Plate reader from Wyatt. A 384-microwell plate was used during the experiment. The results were analyzed using the DYNAMICS software, which accompanies the instrument, and by plotting the received Z-average against temperature.

3.1.3 CD

A temperature ramp of 1°C per min was conducted between 20-90°C using the Chirascan Plus from Applied Photophysics. A sample concentration of 0.1mg/mL and a 0.5mm wide Spectrosil cuvette from Applied Photophysics was used during the far-UV scans, which required a sample volume of 200uL. A

sample concentration of 3mg/mL and a 1mm wide Quartz SUPRASIL cuvette from Hellma Analytics was used for the near-UV scan, which required a sample volume of 300uL. The far-UV scan was conducted between 200-250nm and the near-UV scan was conducted between 250-310nm; an absorbance spectrum was collected at each temperature point for both methods. The results were analyzed using the Global3 software and the wavelengths that absorbed more than 2AU were manually filtered away. Furthermore, the maximum temperature was diminished during the data evaluation if there seemed to be a drastic increase of absorbance in the end of the temperature span, which could be an indication of a drastic change in the sample e.g. due to precipitation.

3.1.4 Probe Drum

A temperature ramp of 1°C per min was conducted between 25-75°C using the Probe Drum from Probation Labs AB and a clear 500uL fluorescence cuvette. Furthermore, a pH titration was conducted where HCl or NaOH was added to the sample. A clear 1000uL fluorescence cuvette was used for the pH titrations. The change in size and shape were measured during all experiments using static light scattering and fluorescence. Absorbance was also measured to track any changes in mAb concentration.

3.1.5 Buffer exchange

Centrifugal filters units called Amicon Ultra – 4 from Merck, with a nominal molecular weight limit of 10,000 and a maximum load volume of 4mL, was used during the buffer exchange. The Minifuge T from Heraeus Christ was used during the buffer exchange. The samples were centrifuged at 3000rpm with an acceleration speed of 7 and a deceleration speed of 5.

3.1.6 NanoDrop

The NanoDrop One from Thermo Scientific was used to measure the concentration in the different samples by measuring the absorbance at 280nm for IgGs. The detection limit is 0.03mg/mL with a reproducibility of ±0.10 mg/mL for samples with a concentration between 0.10 and 10 mg/mL. Hence, the attained concentration was mainly used as a guideline for the approximate sample concentration as the investigated samples had a concentration between 0.005mg/mL and 3mg/mL.

4. Results and Discussion

4.1 Covid-19

It was not possible to fulfill the initial plan as Ferring and the Danish border closed because of the Covid-19 pandemic. Hence, no replicas were conducted on the nanoDSC and the Chirascan that were investigated on Ferring, and few replicas were conducted on the Zetasizer. Yet, the results of the DLS replicas is likely more uncertain than the initial runs as is discussed in section 4.2 and 4.4. It was possible to continue with the investigations on the ProbeDrum and the DynaPro on the Department of Food Technology and Solve after the outbreak, yet no replicas were conducted due to a lack of time. Thus, it was not possible to properly evaluate and validate the methods or the results.

If the outbreak had not occurred, then it would have been desirable to have conducted a minimum of three replicas. A more productive washing method for the Zetasizer would have been investigated and hopefully found. Furthermore, at least one formulation would have been put on a stability study to investigate if the long-term stability corresponds to the predicted stability. The stability study would most likely span over approximately a month, depending on the time available. This data could indicate if one method is better at predicting long-term stability than another.

4.2 Method development

The methods for the five main procedures (DSC, DLS, SLS, CD and intrinsic fluorescence) were investigated including the minimum concentration that could be used to detect mAb in the formulation.

The nanoDSC concentrations that were investigated were 1.0mg/mL, 0.5mg/mL, 0.1mg/mL and 0.05mg/mL NIST mAb in the 25mM Histidine buffer without NaCl. The results can be seen in Figure 7, which shows an overlay graph of the four concentrations of NIST mAb in the 25mM Histidine buffer without NaCl that were investigated. The two highest concentrations have defined peaks whereas the two lowest concentrations do not show any significant peaks. 0.5mg/mL was chosen to be used during the rest of the investigation as it was the lowest investigated concentration that had defined peaks.

It is important to degas the liquid that is investigated using nanoDSC to avoid noisy or incorrect data, and three things were noted that minimized the time needed for degassing. A smaller total volume, a larger water-air interphase and a not completely smooth glass vial minimized the required degassing time. Furthermore, to avoid noisy or incorrect data, the droplets of sample that were often seen on the walls of the nanoDSC wells after the sample transfer could be removed along with any surface air bubbles by tapping the side of the well plate.

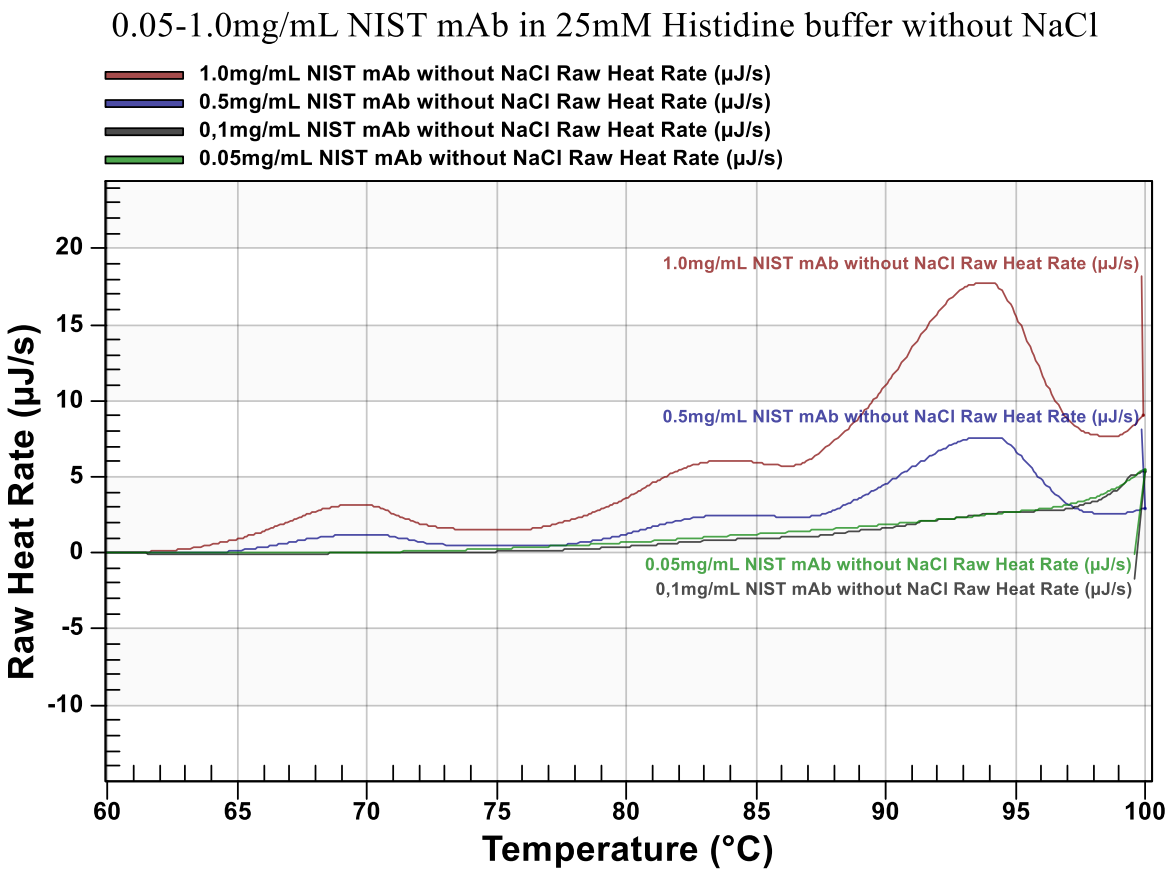

Figure 7. An overlay graph of the four concentrations of NIST mAb in the 25mM Histidine buffer without NaCl that were investigated, namely 1.0mg/mL, 0.5mg/mL, 0.1mg/mL and 0.05mg/mL.

The DLS concentrations that were investigated on the Zetasizer were 0.001mg/mL to 1.0mg/mL NIST mAb in 25mM histidine buffer pH 6 with and without 150mM NaCl, and 0.005 to 0.5 mg/mL NIST mAb in 25mM citrate buffer pH 6.81. The concentrations that were investigated on the DynaPro were 0.1, 0.5 and 1.0 mg/mL NIST mAb in 25mM Histidine buffer pH 6 with and without 150mM NaCl. The Zetasizer could detect mAb at all the investigated concentrations and it chose a laser intensity of 30% for practically all readings, which is an indication of a large amount of scattering and thus large particles in the sample. The DynaPro, similarly to the Zetasizer, conducted a measurement to find the optimal laser intensity for each sample before the reading yet it varied too much from reading to reading at concentrations below 0.5mg/mL NIST mAb. Thus, 0.5mg/mL was the lowest concentration that was used during temperature ramps in the DynaPro.

Water measurements were conducted in the Zetasizer after a couple of scans to assure the reliability of the data. The measurement was conducted as the instrument transfers the sample from the plate to the measurement cell, which increases the risk of cross contamination between the runs. The water measurements indicated that the system was not clean as the scan on MQW gave rise to mass peaks that were very similar to the previously run samples. Note that a DLS measurement on water should not give any types of mass peaks. The mass peaks occurred even though the count rate meter showed that the instrument was clean in between each run. The instrument was thus vigorously cleansed after this discovery by separately pumping NaOH, HCl and 2% Hellmanex alternated with MQW through the system. A scan on pure MQW was run in between each wash but the same correlogram maintained. The tubing was exchanged and the measuring cuvette was removed for cleaning, yet no measurements were run after the cleaning initiation on the Zetasizer as Ferring closed due to the Covid-19 pandemic.

Nevertheless, a freeze-thaw experiment was conducted on the Zetasizer before the outbreak to investigate if freezing could be an appropriate storage method in between each measurement. The experiment was conducted on two samples, one containing 0.1mg/mL NIST mAb in 25mM histidine buffer with 150mM NaCl and the other without NaCl. A scan was conducted on both samples before they were frozen and thawed three times. From this it was noticed that the sample without NaCl had a lot of aggregation, as the sigmoidal curve was not smooth, and it had a correlation coefficient intercept below 0.004. During the three cycles of freezing and thawing it was noticed that it took a slightly longer time for the sample containing NaCl to be frozen. This would be expected due to sodium chloride's effect on water's freezing point. A comparison between the size distribution peaks before and after the three cycles can be seen in Figure 8 and 9 for the sample containing NaCl. From this it can be seen that the size distribution peak included larger particles after the repeated freezing than before. This indicates that the sample with NaCl had aggregated during the repeated freezing and thawing. The sample without NaCl was, as stated previously, aggregated before the freezing and no change in particle size increase could be seen during the experiment. In comparison, it took approximately two weeks after the preparation date until visible aggregation could be seen in the sample with a concentration range of 0.001mg/mL to 0.1mg/mL of NIST mAb in 25mM Histidine buffer pH 6 with and without 150mM NaCl. Due to these discoveries, the storage time in the refrigerator and the number of freeze-thaw cycles were minimized by dividing the 10mg/mL of NIST mAb in 25mM Histidine buffer pH 6 sample into 200uL aliquots. The aliquots were then refrozen and stored in a -80°C freezer until another one was needed for the experiments.

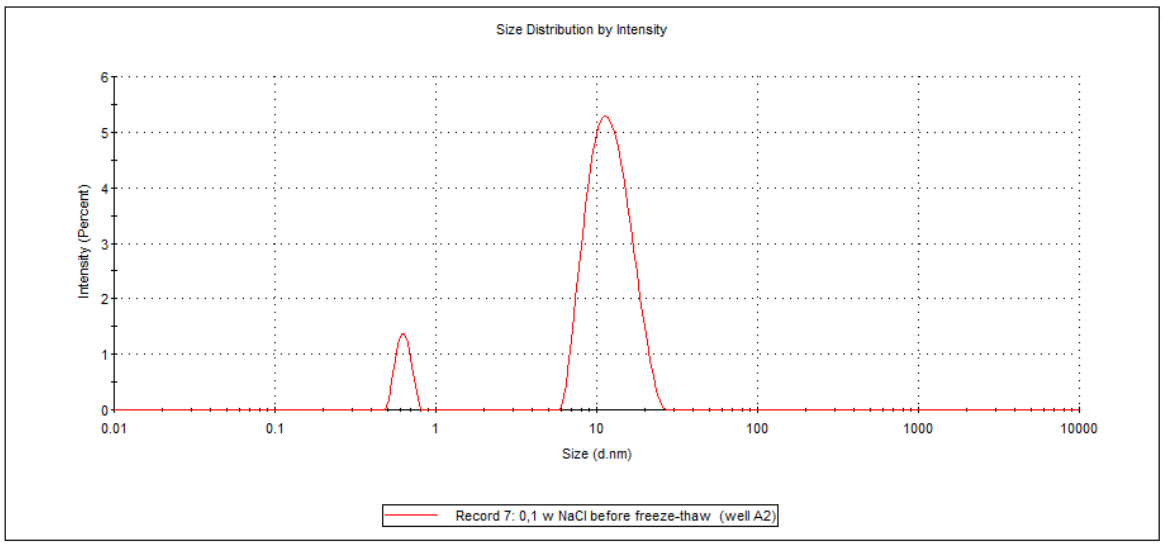

Figure 8. The size distribution of 0.1mg/mL NIST mAb in 25mM histidine buffer pH 6 with 150mM NaCl before freezing and thawing. The first peak is a ghost peak, and most likely a result of the fitting procedure, as other literature values of NIST mAb's hydrodynamic radius was 5.4nm. Hence, it is the second peak in the diagram that is the most interesting.

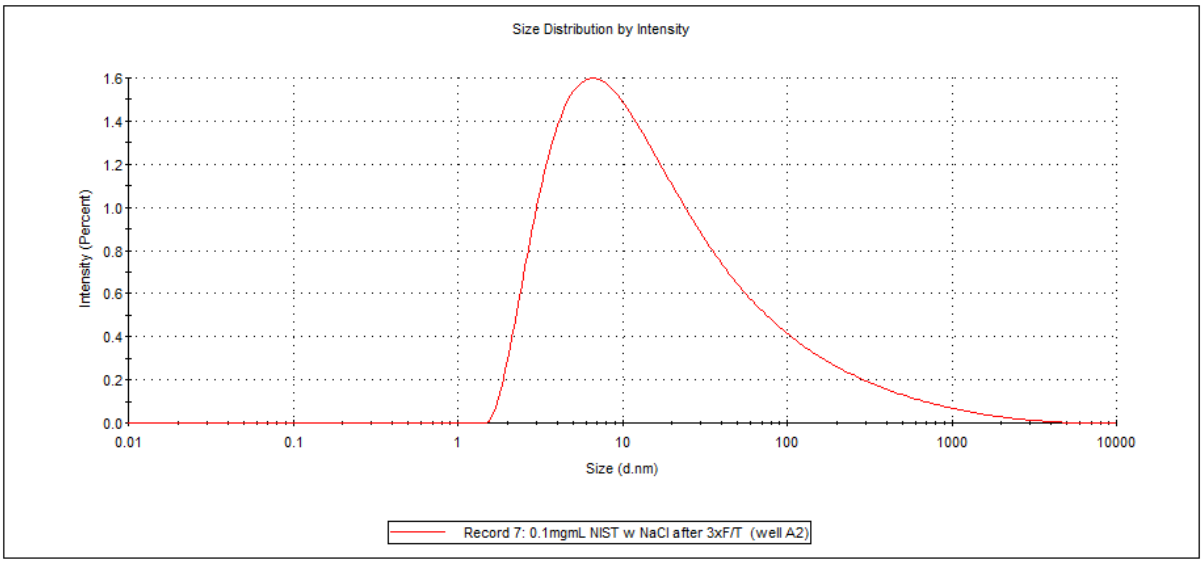

Figure 9. The size distribution of 0.1mg/mL NIST mAb in 25mM histidine buffer pH 6 with 150mM NaCl after freezing and thawing the sample three times.

The CD concentrations that were investigated were 0.1mg/mL in a 0.5mm cuvette for the far-UV and 3mg/mL in a 1mm cuvette for the near-UV. Only one concentration was investigated for each experiment as CD demands a high concentration and a large sample volume. This limited the number of possible trials that could be conducted. The chosen concentrations were recommended by Helen Sjögren and they gave smooth and reliable results after slightly decreasing the scanning rate. The scanning rate of the first and second far-UV scans were 1s per wavelength scan between 190-250nm on the 0.1mg/mL NIST mAb in a 0.5mm cuvette, but it was noticed that the wavelength range was too wide and that results were too jagged as seen in Appendix A1 and A2. The scanning rate for the third scan were thus changed to 2s per wavelength scan between 200-250nm, which resulted in much smoother results, seen in Appendix A3. A lower concentration could possibly be used in both the far- and near-UV measurements but if the same resolution is desired then the wavelength scan rate would have to decrease further. Hence, the concentrations used were 0.1mg/mL in a 0.5mm cuvette for the far-UV and 3mg/mL in a 1mm cuvette for the near-UV.

The SLS and intrinsic fluorescence concentrations that were investigated were 0.005mg/mL to 1.0mg/mL and the concentration of 0.1mg/mL was the lowest concentration that produced data with a good fluorescence signal to noise ratio in the ProbeDrum. Thereafter, the integration time, number of replicas and the measuring span were investigated to find the best settings, for the selected concentration, that does not result in too long runs. The settings that were chosen for all measurements were 5 averages and an integration time of 500ms, with no measurements conducted during equilibrium times. The measurement span for fluorescence was 251-500nm and 600-700nm for SLS. An absorbance measurement over the full absorbance span was conducted to track any changes in mAb concentration.

4.3 DSC

Figure 10 shows an overlay graph of the raw data from the two samples containing 1.0mg/mL NIST mAb in 25mM Histidine buffer pH 6 with and without 150mM NaCl. Three peaks can be seen in the curve of the two samples. The peak position, amplitude and FWHM are similar for the two samples, yet the peaks for the sample containing 1mg/mL NIST mAb in 25mM Histidine buffer with 150mM NaCl

are slightly shifted to the left compared to the peaks of the sample containing 1.0 mg/mL NIST mAb in 25mM Histidine buffer without 150mM NaCl. This shift indicates that the NIST mAb in the sample containing NaCl goes through the configurational changes at a lower temperature, and consequently indicates that NaCl has a destabilizing effect on NIST mAb.

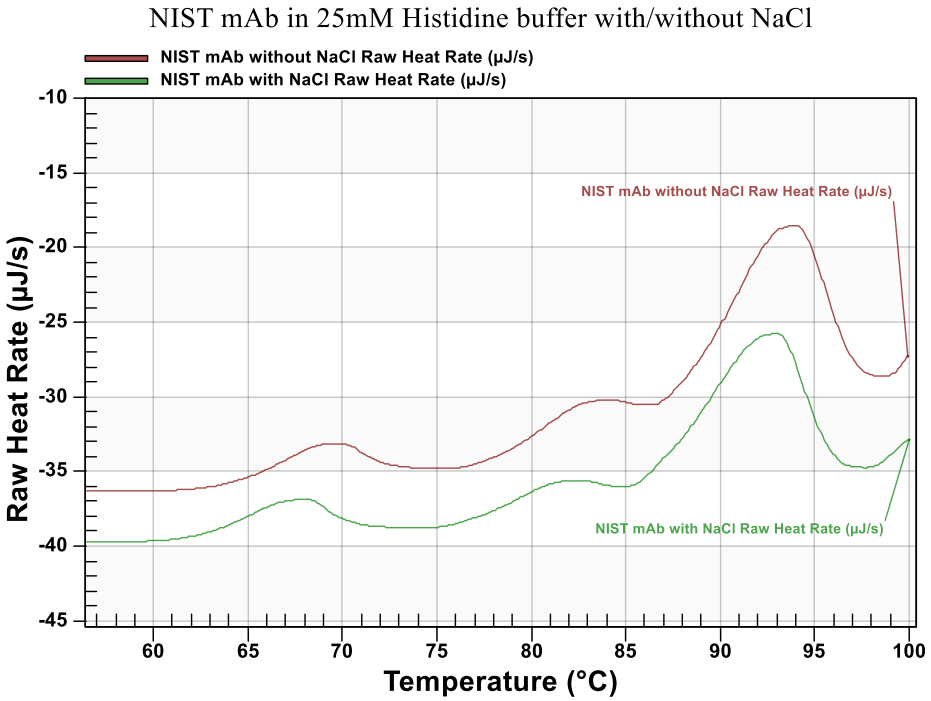

Figure 10. The amount of heat added to the two samples (1.0mg/mL NIST mAb in a 25mM Histidine buffer pH 6 with and without 150mM NaCl) during a temperature ramp between 25-100°C. The reference cell contained the 25mM Histidine buffer at pH 6.

Figure 11 shows the Gaussian model fit to the sample containing 1.0mg/mL NIST mAb in 25mM Histidine buffer without 150mM NaCl, where 25mM Histidine buffer without 150mM NaCl has been subtracted as its blank. A second order polynomial integration baseline is subtracted so that the first peak is baseline separated whereas the second and third are not, which corresponds to the overlay graph of the sample and the blank, see Appendix A4. The model has suggested three different amplitudes, FWHM, peak temperatures, areas and onset temperatures as shown in Figure 11; one for each peak.

The second and third deconvoluted peaks are slightly shifted to the left and does not seem to have the exact same shape compared to the actual peaks. This is true for the DSC data collected for all histidine and citrate solutions independent of pH and tonicity, see Appendix A5, A6, A7, A8, A9 and A10. This means that the FWHM, peak temperatures, areas and onset temperatures shown in the legend are a slightly off. One reason for the shifted deconvoluted peaks is the slight asymmetry of the peaks, which is most visible for the third peak. The program has changed the width and position of the second peak to compensate for the skewed third peak. One suggestion to the asymmetry of the peaks is the irreversible nature of the unfolding, as stated by Freire. Nevertheless, an equilibrium model was assumed during the experiments which is considered to be true if the temperature increase is slow enough to establish an equilibrium between the native and the unfolded state. The asymmetry indicates that the temperature increase was not slow enough at temperatures above approximately 80°C, and that the model was not true above this temperature. This coincides with the data collected

by Gokarn et al. (2015) as mentioned earlier in 2.3.1 DSC where they conducted three different temperature ramps on NIST mAb. The first temperature ramp only surpassed the first conformational change, the second surpassed the two first conformational changes and the third surpassed all three. The study showed almost complete reversibility when only the first configurational change was surpassed and partial reversibility if the second and third conformational change was surpassed. Hence, one cannot assume that there will be an equilibrium between the native and the unfolded state at elevated temperatures. Gokarn et al. (2015) One method of overcoming this problem is to use kinetic models instead of thermodynamic models as irreversible conformational configurations are kinetically driven as stated by Freire (2019).

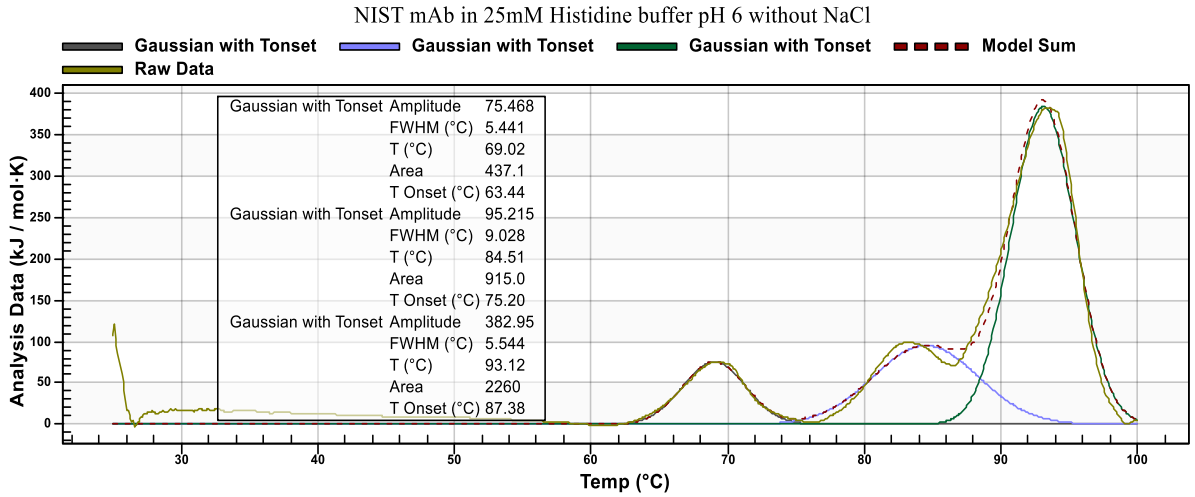

Figure 11. The Gaussian model fit with three peaks for the sample containing 1.0mg/mL NIST mAb in a 25mM Histidine buffer pH 6 without 150mM NaCl. The legend displays the peak amplitude, FWHM, temperature, area and onset temperature. The 25mM Histidine buffer pH 6 has been subtracted as a blank and a second order polynomial has been added as the integration baseline based on the overlay graph of the sample and its blank (A1).

Figure 12 shows the iterated Gaussian model peak amplitude plotted against the T_m for the histidine samples with and without NaCl. The peak position for the three peaks is represented by T_m and each configurational change occurs at approximately the same temperature independent of formulation, which is indicated by the formation of the three clusters in the figure. Nevertheless, there is a slight difference in T_m between the samples with and without 150mM NaCl, where the largest difference is seen for the first peak. The samples without NaCl have slightly higher T_m values which indicates an increased stability. Furthermore, the amplitude of their peaks seems to be slightly higher which further indicates a higher stability as that increases the amount of energy required to complete the configurational change. Additionally, the samples with the lower concentrations have somewhat higher T_m values, which could be an indication that a concentration of 0.5mg/mL NIST mAb is more stable than 1.0mg/mL NIST mAb, or it could be a result of the continuous temperature ramp and the detection limit. The continuous temperature ramp could lead to a peak temperature that is somewhat higher for a sample with a lower concentration as a larger amount, relative to the total amount, of conformational change is required for detection. A conformational change takes some time to fulfill and thus it could be reasoned that the shift that is seen is an effect of this and not an effect of a stability difference between the two concentrations.

Neither the stability of NIST mAb in histidine compared to citrate buffer nor the stability of NIST mAb at different pH follow a similarly clear pattern as the stability of the mAb in a formulation with and

without 150mM NaCl. Figure 13 shows the peak position for 0.5mg/mL NIST mAb in 25mM histidine buffer and 25mM citrate buffer, both at pH 6. The first peak in the graph has a slightly higher T_m in the citrate buffer than in the histidine buffer, but the T_m is slightly lower for second and third peak compared to the values in histidine. If this is true for multiple replicas, then one could change the buffer dependent on which peak stability that is critical, which according to Temel et al. (2016) most likely would be the Fab region. Hence, if the stability of a formulation is dependent on the onset temperature of the Fab peak, then a buffer that maximizes that value can be chosen.

Figure 14 show the peak position for 0.5mg/mL NIST mAb in three citrate buffers at pH 5.0, 6.0 and 6.8. The NIST mAb at pH 5 has the lowest T_m value for the first peak but the highest value for the third peak, whereas NIST mAb at pH 6.8 has the highest T_m value for the first peak and lowest value for the third peak. This information could be similarly used as the peak position dependent on buffer type, if it is true for multiple replicas. Yet, additional data comparisons are required before one could state which peak that has the highest influence on the overall stability, and if T_m or the amplitude has the greatest influence on the stability.

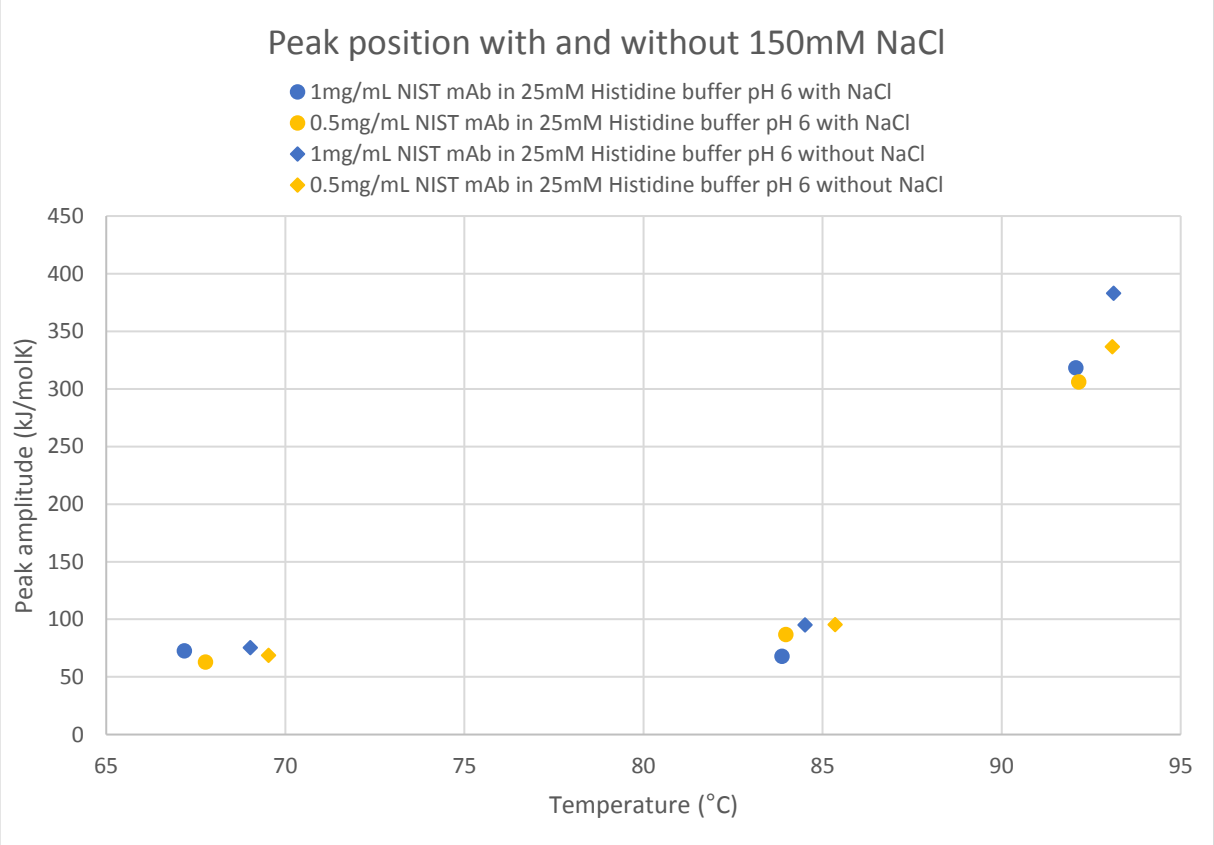

Figure 12. The iterated Gaussian model peak amplitude plotted against the Tm for the samples containing 0.5mg/mL and 1.0mg/mL NIST mAb in 25mM Histidine buffer pH 6 with and without 150mM NaCl.

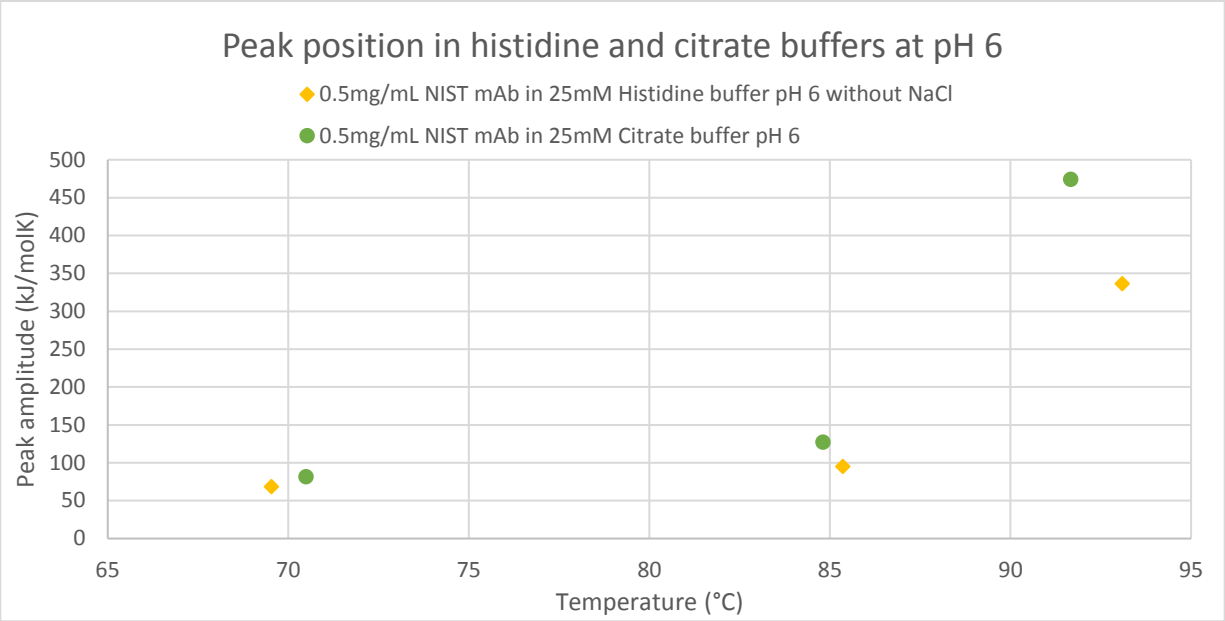

Figure 13. The iterated Gaussian model peak amplitude plotted against the Tm for the samples containing 0.5mg/mL NIST mAb in 25mM Histidine buffer pH 6 and 25mM Citrate buffer pH 6. Neither of the sample contain NaCl.

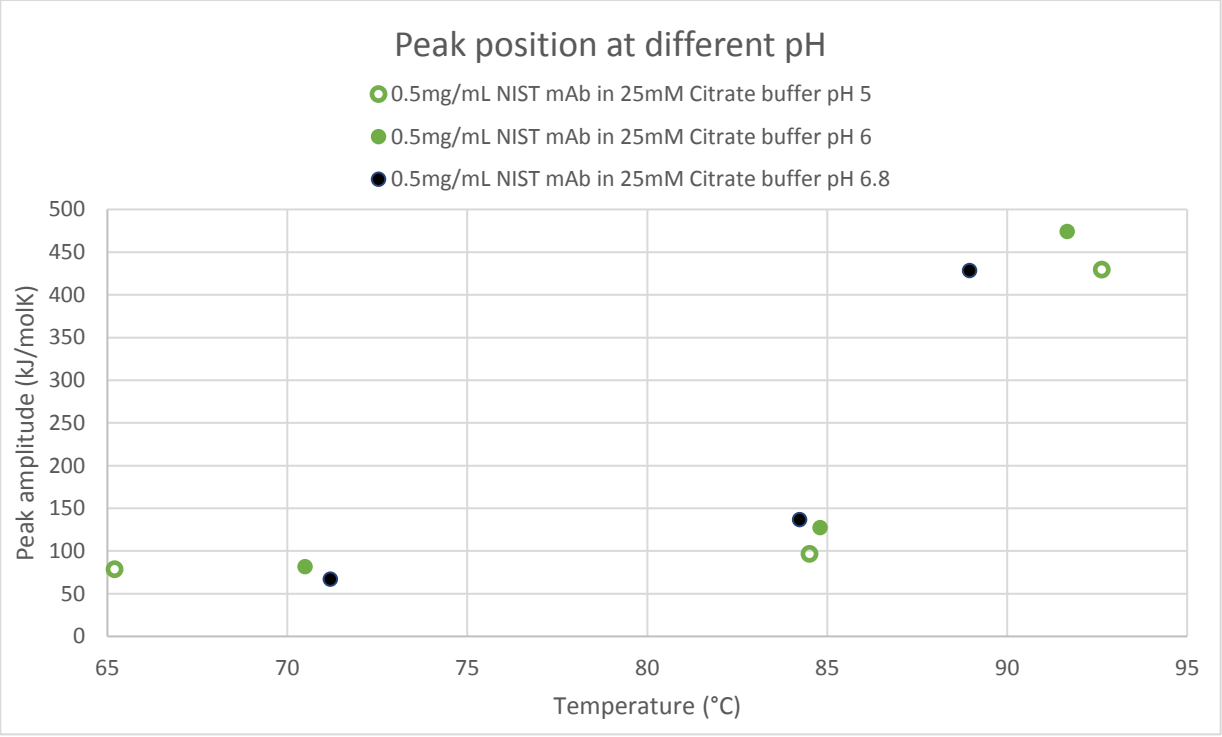

Figure 14. The iterated Gaussian model peak amplitude plotted against the Tm for the samples containing 0.5mg/mL and 1.0mg/mL NIST mAb in 25mM Histidine buffer pH 6 with and without 150mM NaCl.

4.4 DLS

The correlograms from a DLS temperature ramp run can give an initial quick indication of the aggregation temperature (T_{agg}) for each sample without further processing in the Zetasizer. An example of this can be seen in Figure 15, where all the correlograms below 56°C have a similar shape as the sigmoidal curve at 20°C, but an elevated tail can be seen at the sigmoidal curves above 56°C which

indicates a size increase. The elevation is first only slight but then increases to a defined plateau, which can be seen at 76°C. The elevation is detectable by eye in the Zetasizer software whilst scrolling between the correlograms, and the temperature of this initial elevation is very close to the T_{agg} value which is estimated using the calculated Z-average value, see Figure 16. A stepwise temperature increase of 10°C was run on the DynaPro instead of a gradient increase, hence a similar quick estimation of T_{agg} could not be made without further experiments. However, due to lack of time a gradient increase was not conducted on the DynaPro.

The previously mentioned onset of aggregation can be seen in Figure 16 for the solutions containing 0.1 mg/mL NIST mAb in 25mM Histidine buffer pH 6 with and without 150mM NaCl. The solutions had been stored in refrigerated temperatures for zero, six and eleven days; the Z-average was calculated using the built-in analytical algorithm in the Zetasizer software for all measurements except for one which had been calculated using their general algorithm. There is a difference between the calculated Z-average from the two algorithms, and the analytical algorithm gives a steeper Z-average increase that starts at a lower temperature than the Z-average of the general algorithm. Furthermore, the samples that contain NaCl have a lower T_{agg} than the samples without within the same temperature ramp run, which indicates that NaCl destabilize the protein. However, it was noticed during the freeze-thaw experiment, where the samples had been stored for 18 days, that the sample with NaCl had less aggregation than the sample without. This could have occurred due to handling the two samples differently, or it could be an indication that the long-term effect of NaCl in a sample is different than the short-term effect. Yet, more data and a long-term stability investigation would be required before any conclusions can be drawn. As for now, the acquired data do not show a clear pattern between the time spent in storage and the T_{agg}. Yet, the solution that was investigated directly after preparation has the highest T_{agg}, which would be expected as the sample has had less time to form aggregates or aggregation nuclei before the sample was investigated. An increased initial amount of partially unfolded mAb in the solution could increase the aggregation propensity which could arise from storage time or mechanical stress would result in more aggregates at a lower temperature. However, the sample that has been stored for eleven days has a higher T_{agg} than the sample that has been stored for six days, which could be a result of different amounts of stress during the preparation of the sample or during the transfer to the measuring cell.

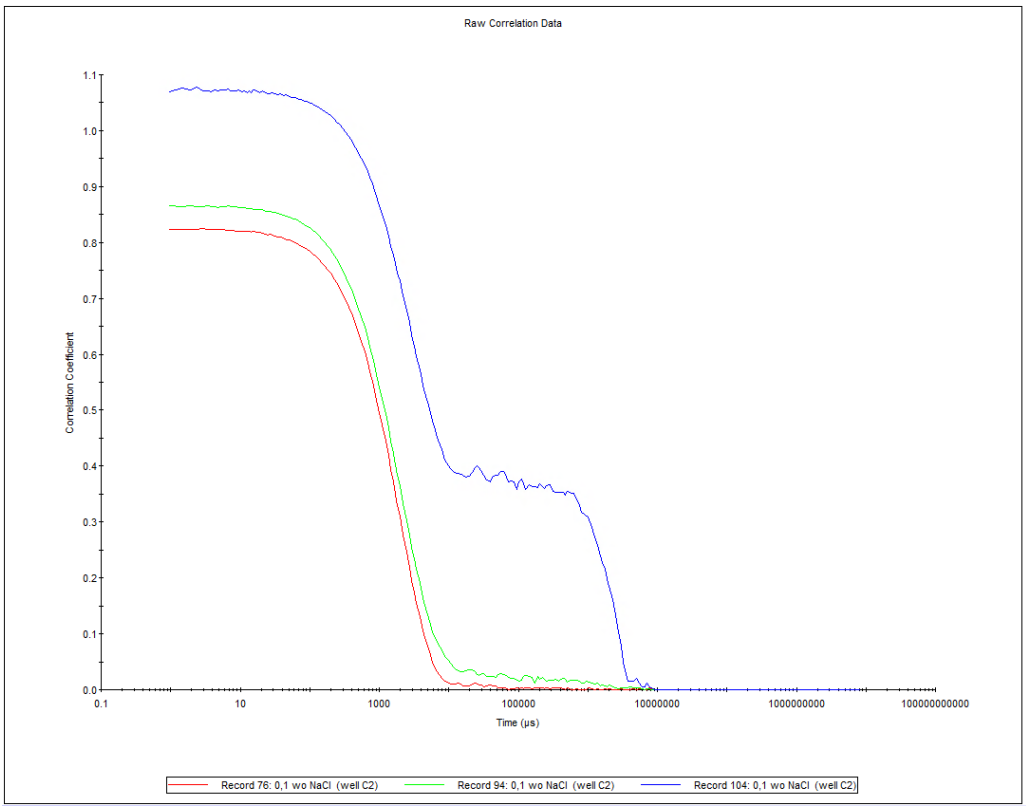

Figure 15. A correlogram showing the correlation coefficient over a short time for 0.1mg/mL NIST mAb in 25mM Histidine buffer pH 6 without NaCl at 20°C (red), 56°C (green) and 76°C (blue).

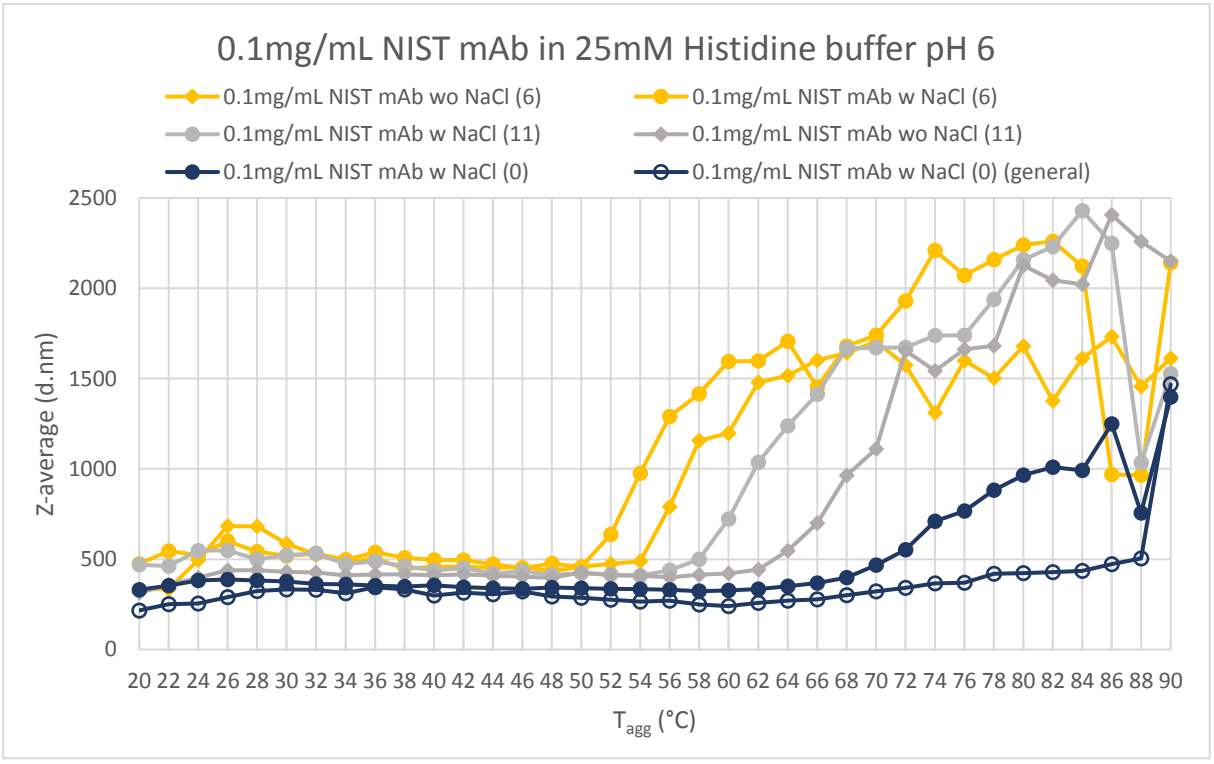

Figure 16. The onset of aggregation for each solution is represented by the drastic increase in size represented by the hydrodynamic diameter, Z-average. 0.1mg/mL NIST mAb in 25mM Histidine buffer pH 6 with and without 150mM NaCl has been investigated after different elapses of time in refrigerated storage. The samples were stored for zero, six and eleven days at 4°C. The Z-average was calculated using an analytical and a general algorithm.

There is a positive correlation between temperature and PdI for the samples that were analyzed with the analytical algorithm in the Zetasizer, which would be expected as the increased temperature leads to more aggregation resulting in a larger spread of the Z-average. However, the PdI trend of the sample that was estimated using the general algorithm had a different trend than the rest, which can be seen in Appendix 11. The correlation between temperature and PdI is a negative correlation for the general algorithm, meaning that the spread of the Z-average should decrease. This can be compared to Figure 16 where the sample that has been analyzed using the general algorithm does not seem to have an as clear aggregation temperature as the other samples. This difference, as stated before, could depend on either a difference in sample handling, transfer or a difference in the algorithm that are used in the instruments' software. Nevertheless, two different algorithms should most likely give similar results if the samples have not been exposed to different amounts of stress. Furthermore, it can be seen that the software in the Zetasizer terminated the temperature ramp for samples that had multiple PdI values of one or zero in a row, see Appendix 12.

There is no clear correlation between the aggregation temperature and the sample concentration for any of the samples that were investigated using the Zetasizer, independent of buffer type (histidine or citrate) and storage time, see Figure 18 and Appendix 13. Neither was there a clear correlation for the samples that were investigated using the DynaPro as no significant Z-average increase could be seen, see Appendix 14. A reason for this could be that the transfer of the solution from the Zetasizer plate to the measuring cell caused mechanical stress on the mAb and induced aggregation, or that it caused an increased amount of surface aggregation. No transfer was conducted in the DynaPro and there was thus most likely less mechanical stress and surface aggregation. Hence, it can be reasoned that the aggregation that is seen in the Zetaziser investigations was not only temperature induced; this is further discussed in section 4.8.

The complete chronological run order on the Zetasizer can be seen in Appendix 15, including each sample's storage time before the sample measurement, the measurement's end temperature and their estimated T_{agg}. The Zetasizer software evaluates the scattering from each measurement at each temperature step in the temperature ramp and terminates the temperature ramp if there is no short-term correlation, meaning that the correlogram is poor. Figure 17 below shows each sample's end temperature, and the sample order is the same chronological order as in Appendix 15. The first three temperature ramp runs are histidine-based samples with and without NaCl, and the fourth to sixth temperature ramp runs are citrate-based samples with and without cooling. The experiments that did not include temperature ramps were excluded, such as the final measurements on MQW and the measurements for the freeze-thaw experiment. From Figure 17 it can be noted that something happened approximately half-way through the third temperature ramp run, at sample number 16, since the end temperature drastically drops. The first sample number in the temperature ramp runs, after the second temperature ramp run, seems to generally have a higher end temperature than the following samples. A possible reason for this is that the Zetasizer cleans the measuring cuvette and the tubing using a standard cleaning wash in between each temperature ramp run that removes residues from the previous runs, which increases the end temperature for the first sample. Yet, as stated in the method development, runs on MQW after the last measured sample and after vigorous cleaning had unexpected mass peaks, which likely arose because of an unclean measuring cuvette and tubing. The state of the measuring cell was confirmed when the instrument was disassembled. Hence, one hypothesis is that a residue of aggregates had been built up on the walls of the measuring cuvette in between the runs. Parts of the residue was cleansed away using the standard cleaning method, yet it

was not vigorous enough to remove it all and this interfered with the scattering of the sample. This interference could possibly affect the accuracy of the results. The hypothesis is further strengthened by the fact that all except one sample's correlation coefficient drops below 0.5 after sample 15, which indicates that the reading is bad as mentioned in the theory.

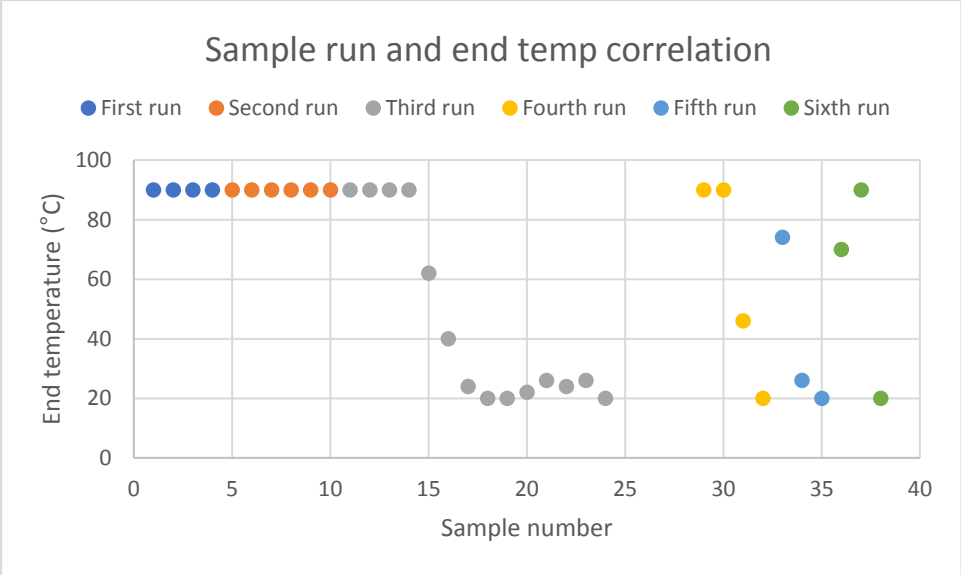

Figure 17. The correlation between the sample number and the temperature ramp's end temperature. Each temperature ramp is color coded and numbered in the measurements' chronological order. Each temperature ramp consists of between three to fourteen samples.

In the fourth and fifth run, where the results likely could be affected by residual scattering, an experiment was conducted to investigate the effect of the cooler on the Zetasizer DLS results. No significant increase in aggregation could be seen as a result of the increased plate temperature for the sample containing 0.005mg/mL NIST mAb pH 6.8. These were the only two samples with the same formulation that could be compared since many of the sample runs were prematurely terminated. It can also be noted that the cooled plate had three samples that exceeded the aggregation temperature, whereas the plate without cooling only had two samples that exceeded the T_{agg}.

There is no clear correlation between the calculated diffusion coefficient and the concentration, the diffusion coefficient and the NaCl concentration of the solution, the diffusion coefficient and the storage time or the diffusion coefficient and the buffer, see Appendix 16 and 17. Furthermore, there seems to be a greater variation of T_{agg} in between the temperature ramp runs than there is between the two types of buffers or the pH, as seen in Figure 18 below. Hence, it cannot be stated that the T_{agg} of the two differently formulated NIST mAb are statistically different with the presented data. More data is required to investigate the above-mentioned correlations as the generated DLS data show great variation, and it would be preferable if the uncertainty concerning the end temperature drop after sample 15 could be solved.

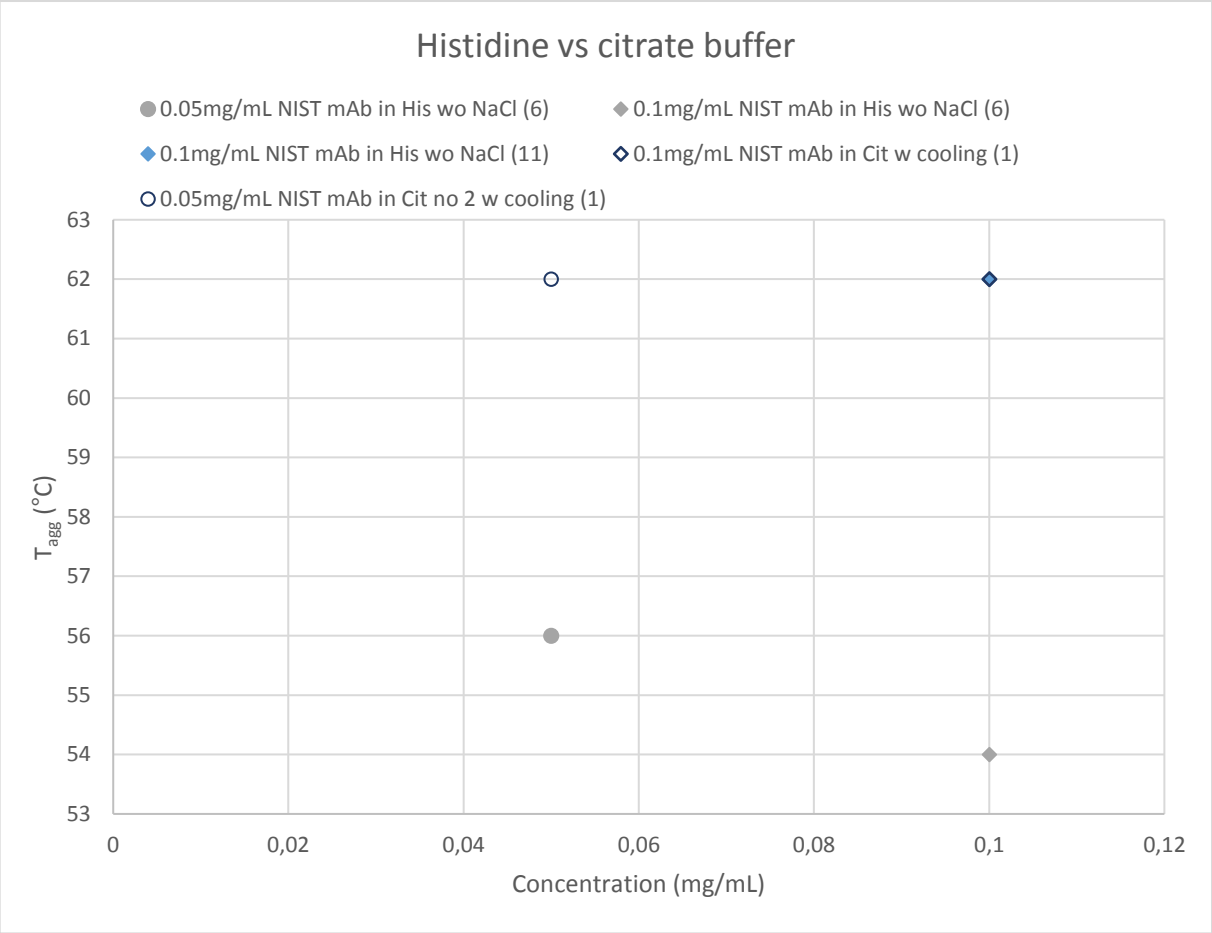

Figure 18. The T_{agg} for two different concentrations of NIST mAb in both 25mM Citrate buffer pH 6.8 and 25mM Histidine buffer pH 6.

The calculated Z-average for the samples at all the investigated temperatures on the DynaPro ranged from approximately 5.4nm to 8.5nm and the average of this was 5.9nm, which is much lower than the Z-average calculated by the Zetasizer. This value is very similar to the value of 5.4nm that J. Schiel et al (u.d.) received during their measurements. The Z-average for all the investigated temperatures is illustrated in Figure 19 and the calculated Z-average seems to be rather stable over the different temperatures, which indicates that it mainly contains the monomer population. There are readings with an elevated value, which could be a measurement of dimers in the sample. However, they are not consistent over temperature which could indicate that the dimerization is reversible. A reason to why no aggregation could be seen is because the temperature ramp ended below T_{agg}. It is unlikely that the exposure to the elevated temperatures was too short as the step wise temperature increase took approximately 3 hours.

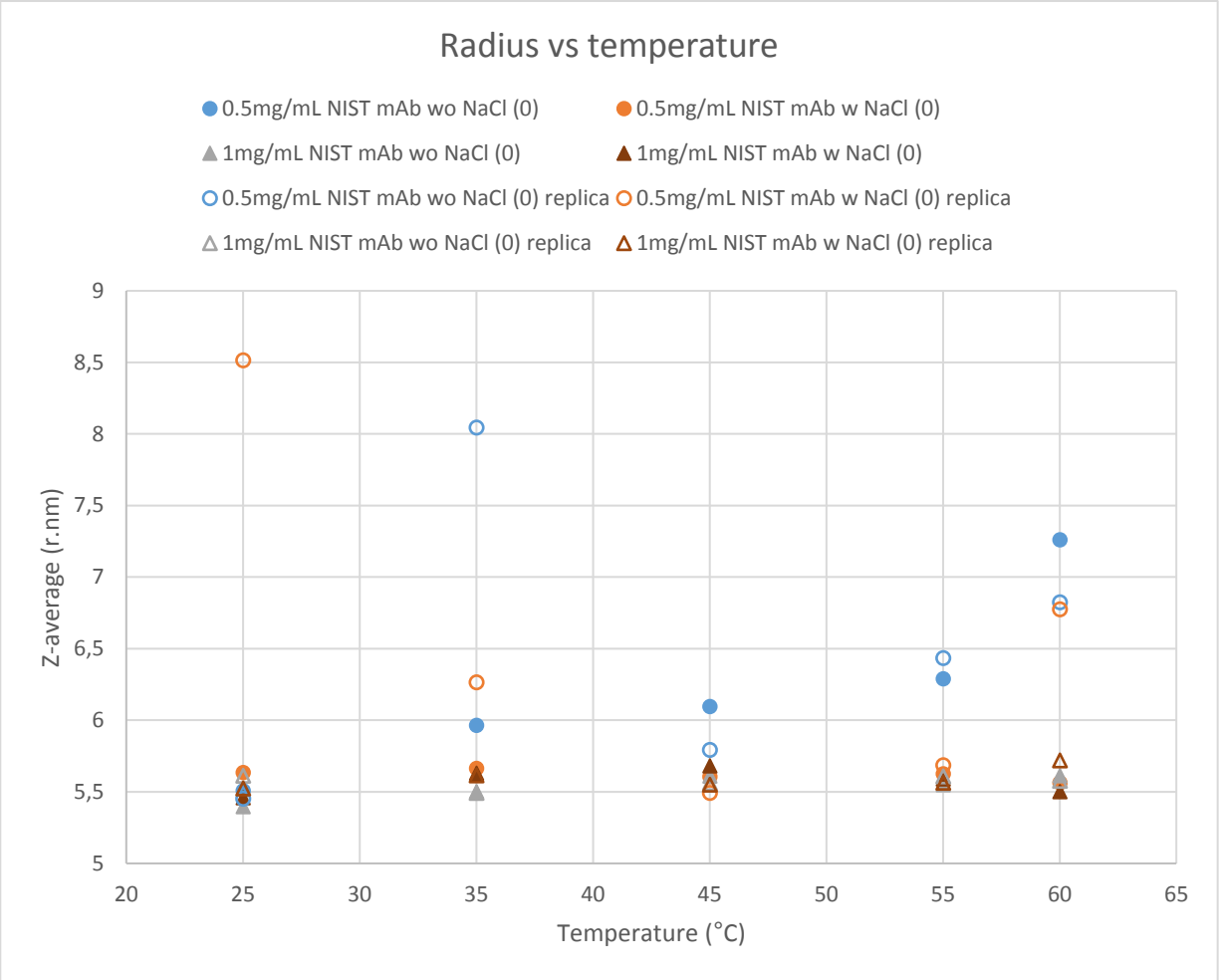

Figure 19. The calculated hydrodynamic radius, Z-average, at each investigated temperature in the DynaPro.

4.5 CD

The calculated far-UV spectra for the three transition states that occur when NIST mAb in 25mM citrate buffer at pH 6.8 is heated in a temperature ramp between 20-90°C is seen in Figure 20 below. The native state has a maximum at approximately 203nm and a minimum at 218nm which indicates that it mainly is constituted by beta-sheets in this formulation and at this temperature. The first transition state has the same shape as the native state but a lower magnitude. The second transition can only be partially seen in this temperature range, the calculated peak position occurs at 89.5°C as seen in Table 3, and this could be a reason why the spectra of the second transition looks rather flat. Nevertheless, a slight minimum can be seen in the raw data at approximately 205nm at the elevated temperatures during the temperature ramp, which corresponds to a random coil. The acquired spectra at pH 5 is similar to the spectra at pH 6.8, however the native and first transition are positioned closer to each other and the second transition has a more defined trough at 205nm, see Appendix 18.

The calculated near-UV spectra for the two states that occur when NIST mAb in 25mM citrate buffer at pH 6.8 is heated in a temperature ramp between 20-90°C is seen in Figure 21 below. The native state has a greater magnitude than the first transition state in the 250-300nm region, but the finer features in the spectra remains throughout that region. This indicates that it is mainly the disulphide bonds that move. The spectra were not collected for wavelengths above 310nm, yet it could give

further information about the disulphide bond movement and possible precipitation. The acquired spectra at pH 5 and 6 are very similar to pH 6.8, however the fine features between 275-282nm is slightly changed which indicates that the environment surrounding tyrosine might have changed, see Appendix 19 and 20. Furthermore, there is a decrease relative to the native structure above approximately 300nm, which could be a second result of the disulphide movement.

An interesting observation during the CD-experiments was that stringy aggregates could be seen after the temperature ramp on the 3mg/mL NIST mAb samples, but it could not be seen in the 0.1mg/mL NIST mAb samples. It would be reasonable that the aggregate can be seen due to the concentration difference.

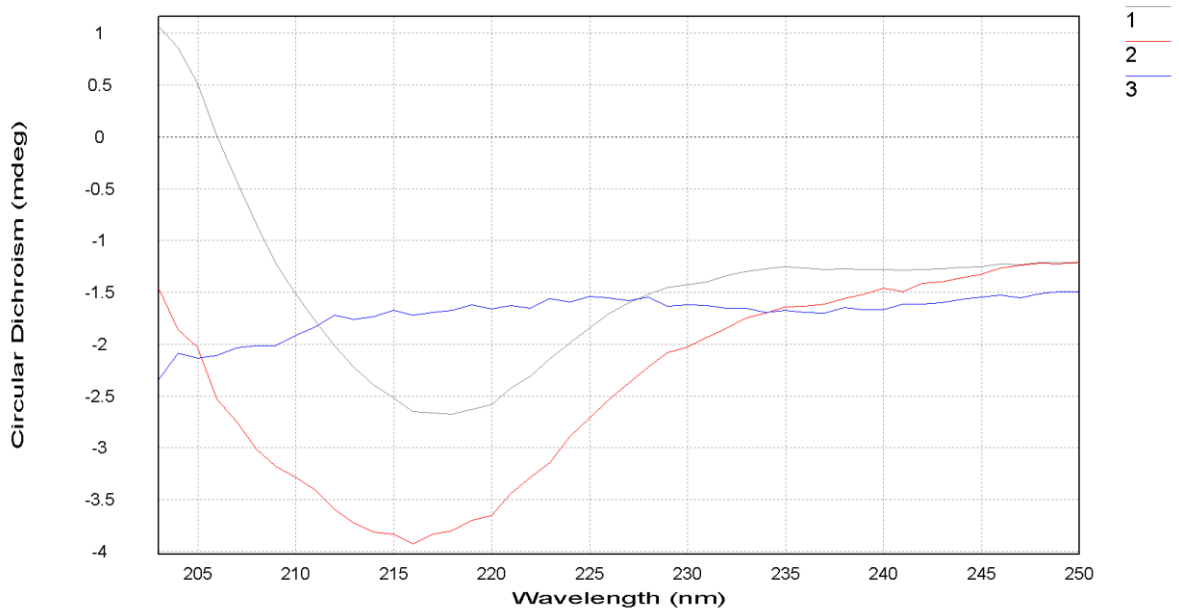

Figure 20. The calculated far-UV spectra for the three states that occur when NIST mAb in 25mM citrate buffer at pH 6.8 is heated in a temperature ramp between 20-90°C. The native state is named 1, the first transition state is named 2 and the second transition state is named 3.

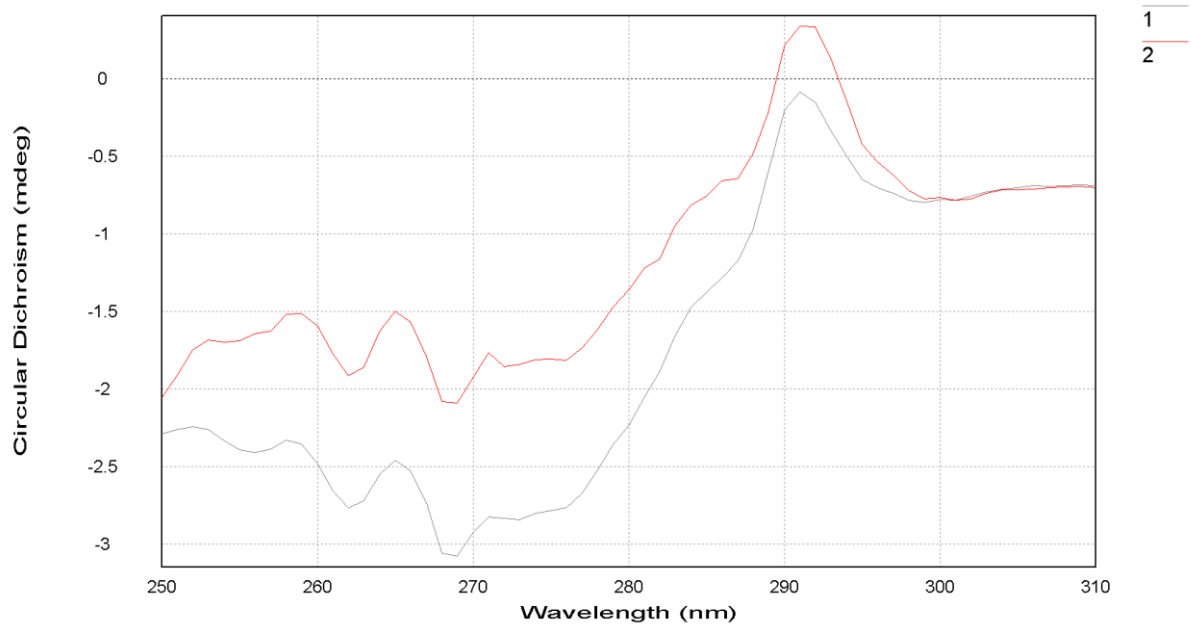

Figure 21. The calculated near-UV spectra for the two states that occur when NIST mAb in 25mM citrate buffer at pH 6.8 is heated in a temperature ramp between 20-90°C. The native state is named 1 and the first transition state is named 2.

The melting temperatures calculated through Global3, for both the far-UV and the near-UV spectra, for the three citrate formulations with pH 5, 6 and 6.8 are seen in Table 3. The residual values did not converge to an acceptable minimum for the solution with pH 6 during the fitting of the near-UV spectra, and thus they are excluded in Table 3 and Figure 22. Figure 22 shows the correlation between the melting temperatures of each peak in the far- and near-UV spectra and the formulation pH. In the investigated pH-span there seems to be a positive correlation between the temperature and the pH. This is slightly surprising as the higher pH is closer to NIST mAb's pI and it would then be reasonable that the overall charge would decrease, which would lead to an increased amount of aggregation which is a type of conformational change. Furthermore, it can be seen that the second peak in the far-UV spectra has the highest melting temperature and that the first peak in both the far- and near-UV seems to have rather similar melting temperatures compared to each other.

Table 3. The resulting melting temperatures for a far-UV and a near-UV CD scan run on NIST mAb in three formulations with different pH.

	Far-UV		Near-UV
	Temperature (°C)		Temperature (°C)
	Peak 1	Peak 2	Peak 1
0.5mg/mL NIST mAb in 25mM Citrate buffer pH 5	58.0	77.5	61.3
0.5mg/mL NIST mAb in 25mM Citrate buffer pH 6	-	-	67.9
0.5mg/mL NIST mAb in 25mM Citrate buffer pH 6.8	72.9	89.5	69.2

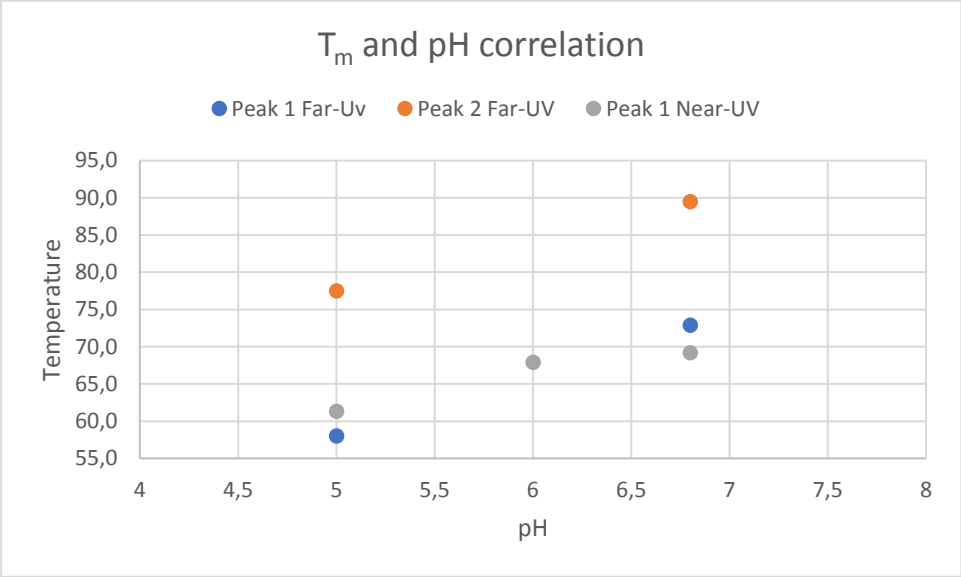

Figure 22. The correlation between the melting temperature and the pH of the formulation, for a far-UV and a near-UV CD scan run on NIST mAb.

4.6 SLS

The SLS measurements only showed the excitation peak at 636nm. Hence, no aggregation could be detected during the investigated conditions. It could possibly be an effect of the low mAb concentration.

4.7 Intrinsic fluorescence

The intrinsic fluorescence signal for the tryptophan peak, which appeared in the interval between approximately 326-348nm, decreased in a slightly polynomial manner between 25 to 72°C, see Figure 23. In the same temperature span the peak of that signal shifted from 335.4nm to 332.2nm at 64°C, see Figure 24. This can be compared to the literature emission value of 348nm and it can be concluded that Trp exists in a more polar environment in both states. Furthermore, it can be noted that a type of unfolding probably occurs at 64°C as the wavelength decreases by approximately 3nm. The absorbance spectra had the expected absorbance peak at the excitation wavelength of 280nm, and it fluctuated randomly around approximately 0.1, which indicates the concentration was too low for absorbance measurements and that no absorbance change could be noted.

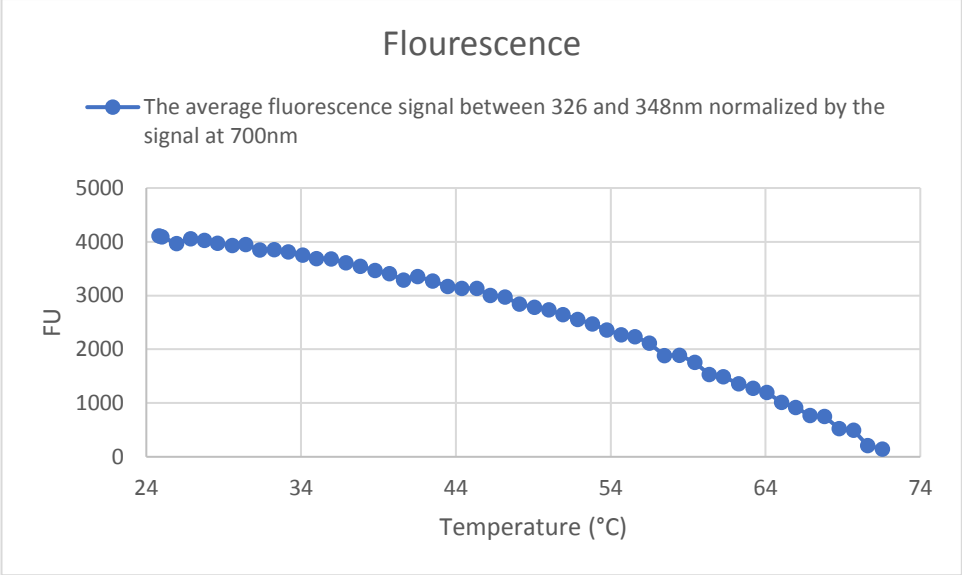

Figure 23. The average tryptophan fluorescence signal for 0.1mg/mL NIST mAb in 25mM Histidine buffer pH 6 between 326 and 348nm normalized by the signal at 700nm, which was a part of the baseline, in the temperature span of 25 and 72°C.

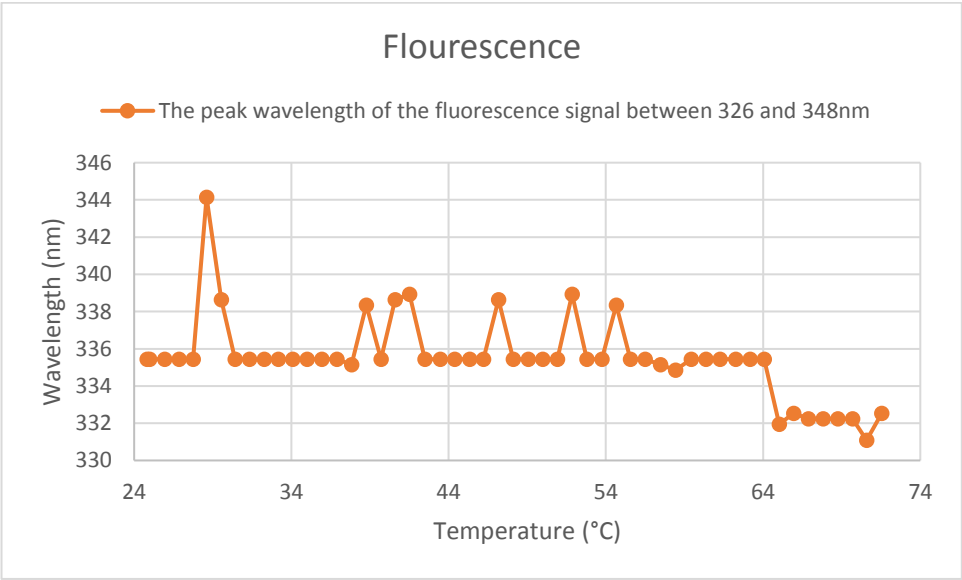

Figure 24. The peak wavelength of the tryptophan peak between 25 and 72°C for 0.1mg/mL NIST mAb in 25mM Histidine buffer pH 6.

The average fluorescence signal at approximately 326-348nm varied rather randomly around approximately 420nm during the pH titrations as seen in Figure 26. Yet, there seems to be a peak value

around pH 6.38 which was the starting pH where either HCl or NaOH was titrated into the solution. This same disruption is seen in Figure 27 as a signal drop. Figure 27 displays Trp's fluorescence peak wavelength during the titrations and a slight wavelength shift from 336.9nm at pH 5.2 to 337.8nm at pH 5.7 can be noted in the figure. This can be an indication that Trp moves to a more polar environment when the pH is decreased to 5.2. Figure 28 displays the average absorbance signal at 276-286nm relative to the baseline at 700nm. There seems to be a slight negative trend in the pH span and it is localized around 0, which indicates that the concentration was too low for absorbance measurements and that the Trp absorbance decreased slightly with an increase in pH.

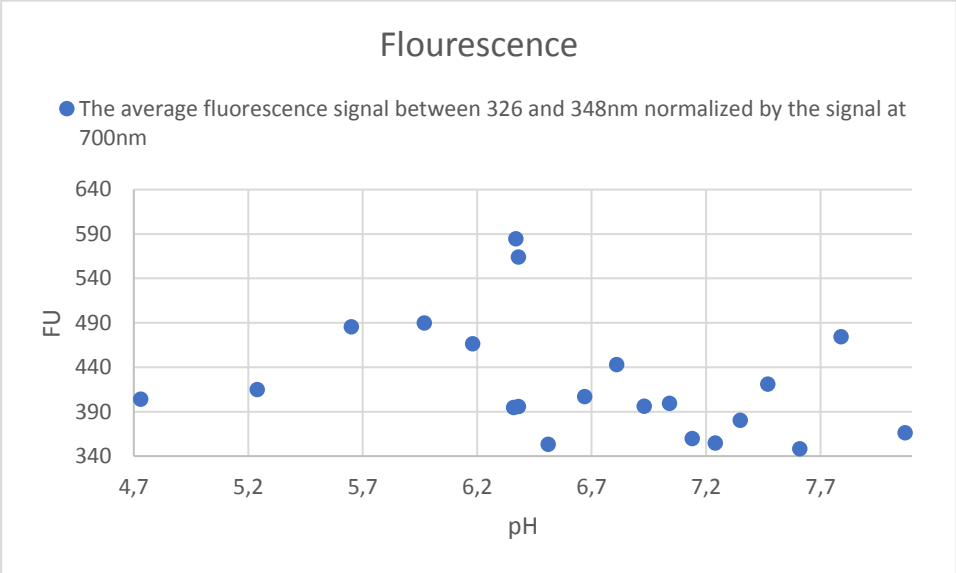

Figure 26. The average tryptophan fluorescence signal for 0.1mg/mL NIST mAb in 25mM Histidine buffer pH 6 between 326 and 348nm normalized by the signal at 700nm, which was a part of the baseline, in the pH span of 4.7 to 8.1.

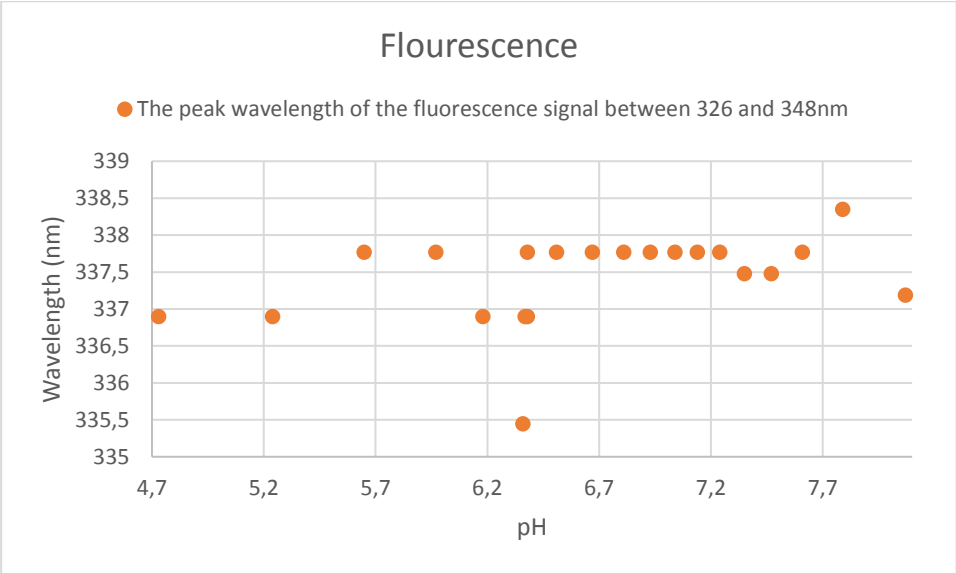

Figure 27. The peak wavelength of the tryptophan peak in the pH span of 4.7 to 8.1 for 0.1mg/mL NIST mAb in 25mM Histidine buffer pH 6.

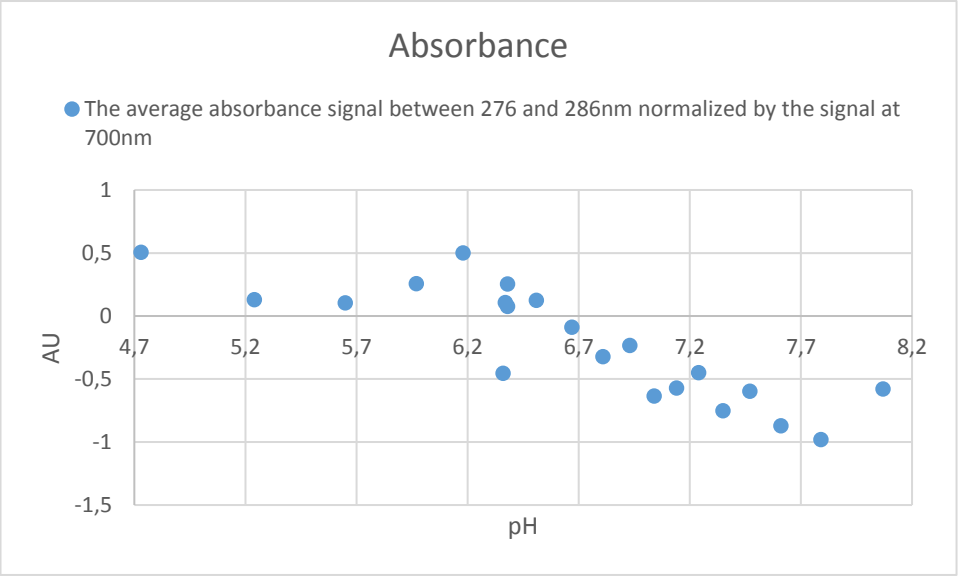

Figure 28. The absorbance of tryptophan's excitation wavelength, 280nm, compared to the baseline at 700nm between pH 4.7 to 8.1.

4.8 Comparison between DSC, DLS, CD and intrinsic fluorescence

The peak temperature for any conformational change that occurs during the temperature ramps for the samples containing 0.5mg/mL NIST mAb in a 25mM Histidine or Citrate buffer are compared for the DSC, DLS, CD and fluorescence data. This is visualized in Figure 29 to see if the different measuring methods detect the same or different conformational changes. The position on the x-axis in Figure 29 is important as it represents the peak temperature for any conformational change for that method and each marker represents the measurement for one sample. Figure 29 shows that the conformational changes that occurred at the highest temperatures can be seen using the DSC, where the second and third peak lies higher than most of the conformational changes recorded by the other techniques. An exception to this is the second peak in the far-UV spectra from the sample containing a citrate buffer at pH 6.8, which lies above the second DSC peaks. The other techniques for measuring the conformational changes overlaps each other in the span of 54-78°C. This could be an indication that the CH_2 region in the mAb plays an important role in the conformational stability of the antibody during a temperature ramp since most instruments detects it as the start of a conformational change and aggregation. It questions the idea that the Fab region gives a better indication of the stability than the other regions, nevertheless it might true for a long-term stability which might differ from a short term thermally induced conformational change.

The technique that recorded the lowest conformational change was the DLS measurement, which noted a size increase at 54°C for the sample that contained 0.5mg/mL NIST mAb in a histidine buffer with 150mM NaCl at pH 6.0. Hence, the order of these techniques as seen in Figure 29, from lowest to highest peak temperature for any conformational change, is DLS, far-UV peak 1, near-UV peak 1, blue shift in fluorescence wavelength, DSC peak 1, far-UV peak 2, DSC peak 2 and DSC peak 3. This can be simplified to state: DLS, CD, intrinsic fluorescence and DSC.

The low T_{agg} that was recorded by the Zetasizer raises some questions since it would be reasonable that the recorded conformational changes would occur after the aggregation temperature. A reason for the observations could be that the aggregation that is seen in the DLS measurements in the Zetasizer is not only caused by conformational changes but could be due to other stress inducing factors such as mechanical stress and an increased amount of surface induced aggregation during

pumping. Furthermore, one should take into consideration the effect that a temperature ramp could have on the registered conformational peak temperature during the DSC, DLS, CD and fluorescence measurements, as it might be overestimated. A shift can be an effect of a continuous temperature ramp and the instrument's detection limit, as the conformational change occur gradually over a time-period. This could affect all the methods.

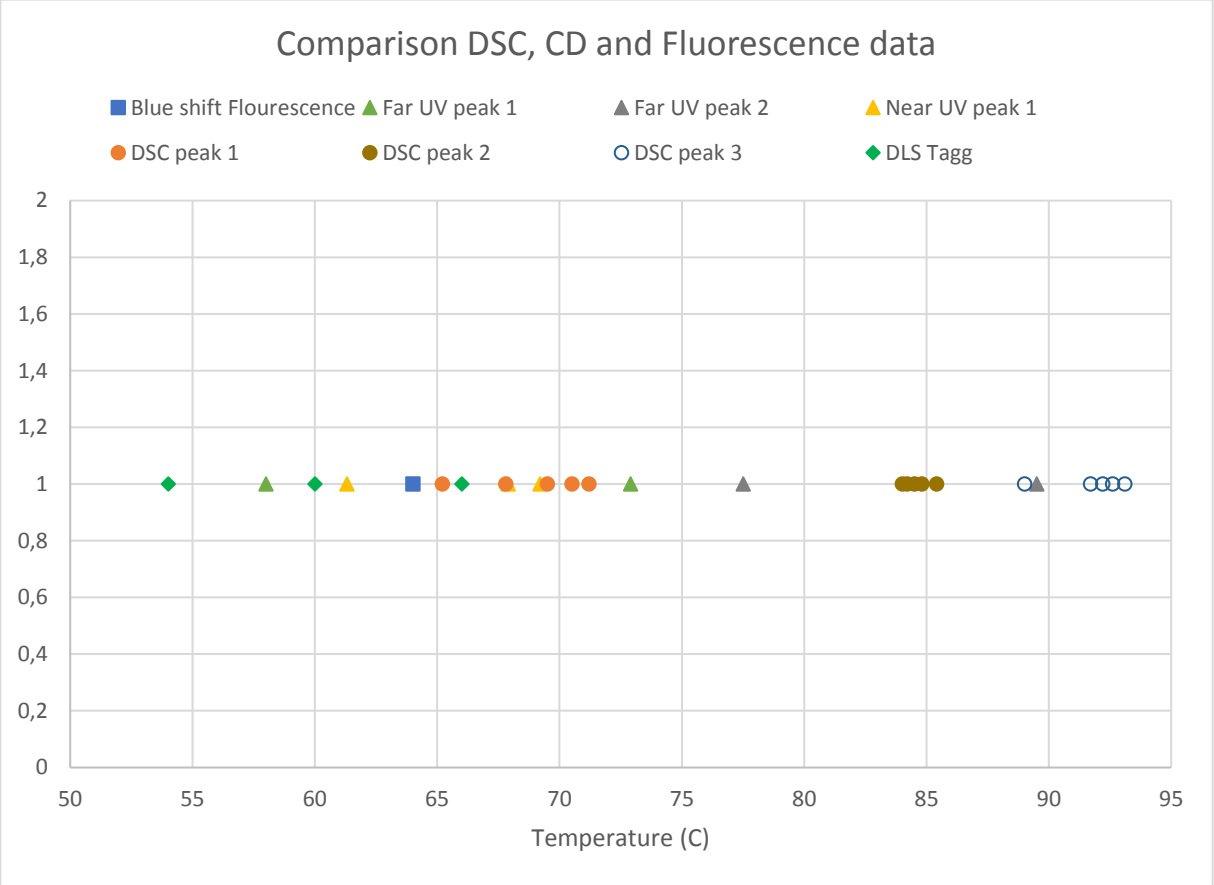

Figure 29. The temperatures where conformational changes and aggregation of 0.5mg/mL NIST mAb in 25mM Histidine or Citrate buffer was registered by DSC, DLS, CD and intrinsic fluorescence.

It is difficult to assess the applicability of the investigated methods and instruments, whilst taking the limited amount of collected data into consideration, as they are quite different, and all have a great potential if used correctly. For example, the Zetasizer and the DynaPro uses very little material but they are very sensitive and can thus be easily affected by different types of material handling. It would be discouraged to use a DLS instrument that pumps the sample due to an increased risk of stress and possibly cross-contamination dependent on the sample flow in the tubes. It would thus be more preferable to use a plate reader as DLS measured size change which could a result of many factors. The fluorescence measurements in the ProbeDrum required more material than the investigated DLS instrument yet less than the nanoDSC or the Chirascan if a small fluorescence cuvette is used. It is however good to note that the ProbeDrum would require a higher concentration than the one used in the investigations to acquire SLS measurements, and to achieve less spikey absorbance and fluorescence data than acquired. The nanoDSC required less material than the near-UV measurements in the Chirascan and is a rather robust technique as it measures the heat required that is used for the conformational change. The Chirascan and fluorescence measurements could have a very interesting applicability as it could detect conformational changes at comparatively low temperatures, as seen in Figure 29. As aforementioned Gokarn et al. (2015) investigated and noticed an almost complete reversibility for temperatures that only reached the first DSC peak, and if this information is applied

then one could possibly reuse mAbs in investigational methods that do not exceed that temperature. CD and fluorescence measurements are the two methods that note conformational changes below the temperature of the first DSC peak and could possibly be considered to be used in such a manner.

Nevertheless, the different instruments detected different formulation changes. The nanoDSC noticed a change in stability when comparing a solution with and without 150mM NaCl. This was also true for the samples that were investigated with the Zetasizer, when comparing the results of the same run. It was not investigated for the Chirascan and the ProbeDrum due to a lack of time. The stability changes due to pH changes could be detected by DSC, CD and fluorescence, but it is not clear if DLS could detect a stability change based on the received results. The stability changes due to buffer changes are unclear for all the measurements.

5. Conclusion

The instruments detect different conformational changes as they investigate different parts of the mAb and they received different peak temperatures of the conformational changes. Most instruments detect conformational changes in the span of 54-78°C, and the order of the instruments from lowest to highest first peak temperature for any conformational change is: DLS, CD, intrinsic fluorescence and DSC. However, the conformational changes that were detected for the DLS were most likely influenced by a mechanical stress that occurred during the transfer to the measuring cell, which decreased the aggregation temperature.

The addition of salt was investigated using the nanoDSC and the Zetasizer and it was noticed that it caused destabilization of the mAb in both cases. This is likely due to the shielding effect that is caused by the ions that mask the repulsion of the ionic surface. The effect of pH on the mAb was investigated using DSC, DLS, CD and fluorescence. The CD measurements shows a positive linear trend between stability and pH for the investigated solutions, and a slight wavelength shift was detected during the fluorescence measurements between pH 5.2 and 5.7. The positive trend is slightly surprising as a pH closer to the mAb's pI often lead to a more aggregation prone mAb, thus having a lower stability. The shift could indicate that Trp moves to a more polar environment when the pH is decreased to 5.2. Yet, the trend was not as clear for the DSC since the peak position at pH 5 was wider than at pH 6 and 6.8, and the peak position at pH 6.8 was the narrowest. This means that the first peak at pH 5 had the lowest stability and the last peak had a highest stability, and the first peak at pH 6.8 had the highest stability but the lowest stability for the last peak. Furthermore, it is not clear if DLS could detect a stability change based on the received results. Lastly, there are no clear correlations between the buffer types and the mAb stability for any of the investigated methods. Thus, it can be concluded that the methods detect different formulation changes, yet it is difficult to determine which investigational method is the most applicable in early formulation development.

6. Future work

Further studies could include the same methods but other commonly used excipients such as sucrose, surfactants and amino acids. These was considered in the initial plan but NaCl was chosen as the excipient that was going to be investigated first and the other excipients were not investigated due Covid-19 which caused changes in the initial planning. These studies would further deepen the understanding if one method is better at noting the stability change that occurs during the addition of the excipients and if that addition has a linear correlation with stability or a more complex correlation. Furthermore, one could compare two antibodies to see if these react similarly to the addition of excipients or if there is a variation between the antibodies. The comparison would also give an insight if one method is better at detecting the stability differences between antibodies.

Additionally, reversibility studies such as those mentioned by Gokarn et al. (2015) could be conducted, where the sample is heated to a certain temperature and then set aside to cool to regain its native conformation. This could give insights on how the reversibility is affected by different formulations and if it is closely related to the long-term and the predicted stability. Moreover, the reversibility studies could be used to see if the material that is used in certain methods, that note conformational changes at a relatively low temperature, can be re-used in a second measurement. This would be interesting to investigate as only a limited amount of mAb is available in the early formulation development.

Lastly, it would be interesting to acquire more DSC data to see if the Fab peak has the greatest influence on the mAb stability as stated by Temel et al. (2016), and if so one could compare how different formulations affect the Fab region's stability. Furthermore, it would be interesting to know if it is the peak position or the amplitude that has the greatest influence on the stability.

References

Aldrich, S., 2020. *NISTmAb, Humanized IgG1k Monoclonal Antibody.* [Online]
Available at: https://www.sigmaaldrich.com/catalog/product/sial/nist8671?lang=en&region=DK
[Accessed 18 May 2020].

Applied Photophysics, 2012. *User Manual Chirascan Series Spectrometers.* s.l.:s.n.

Applied Photophysics, 2019. *Beyond α-Helix and β-Sheet: the Expanding Role of Circular Dichroism.* [Online]
Available at:
https://www.photophysics.com/assets/media/Circular%20Dichroism/The%20Expanding%20Role%20of%20Circular%20Dichroism%20White%20Paperv2.pdf?su=/circular-dichroism/chirascan-technology/white-paper/
[Accessed 18 May 2020].

Applied Photophysics, 2020. *Circular Dichroism Units and Conversions.* [Online]
Available at: https://www.photophysics.com/circular-dichroism/chirascan-technology/circular-dichroism-spectroscopy-units-conversions/
[Accessed 18 May 2020].

Aulton, M. E., 2007. *Aulton's Pharmaceutics: The Design and Manufacture of Medicines.* 3rd ed. s.l.:Elsvier.

Bahrenburg, S., Karow, A. R. & Garidel, P., 2015. Buffer-free therapeutic antibody preparations provide a viable alternative to conventionally buffered solutions: from protein buffer capacity prediction to bioprocess applications. *Biotechnology Journal,* 10(4), pp. 610-622.

Brange, J., 2000. Physical Stability of Proteins. In: S. Frokjaer & L. Hovgaard, eds. *Pharmaceutical Formulation Development of Peptides and Proteins.* s.l.:CRC Press, pp. 89-112.

Chiralabs, 2020. *Circular Dichroism Applications: Protein Structure Analysis. Near-UV.* [Online]
Available at: https://www.chiralabsxl.com/Circular_Dichroism/CD_App_Protein_NUV.html
[Accessed 11 May 2020].

Drugs.com, 2020. *Sodium Chloride Injection.* [Online]
Available at: https://www.drugs.com/pro/sodium-chloride-injection.html
[Accessed 18 May 2020].

Freire, E., 2019. Can calorimetry provide accurate estimates of long-term stability of monoclonal antibodies?. *European Pharmaceutical Review,* Issue 4.

Gervasi, V. et al., 2017. Parenteral protein formulations: An overview of approved products within the European Union. *European Journal of Pharmaceutics and Biopharmaceutics,* Volume 131, pp. 8-24.

Ghisaidoobe, A. B. T. & Chung, S. J., 2014. Intrinsic Tryptophan Fluorescence in the Detection and Analysis of Proteins: A Focus on Förster Resonance Energy Transfer Techniques. *MDPI,* 15(12), pp. 22518-22538.

Gokarn, Y. et al., 2015. Biophysical Techniques for Characterizing the Higher Order Structure and Interactions of Monoclonal Antibodies. *ACS Symposium Series,* Volume 1201, pp. 285-327.

Gokarn, Y. R. et al., 2008. Self-buffering antibody formulations. *Journal of Pharmaceutical Sciences,* 97(8), pp. 3051-3066.

Helmenstine, A. M., 2019. *Amino Acid Chirality.* [Online]
Available at: https://www.thoughtco.com/amino-acid-chirality-4009939
[Accessed 18 May 2020].

Le Basle, Y. et al., 2019. Physiochemical Stability of Monoclonal Antibodies: A Review. *Journal of Pharmaceutical Sciences,* 109(1), pp. 169-190.

Malvern Instruments, 2015. *Malvern Instruments - Static Light Scattering technologied for GPC - SEC explained.* [Online]
Available at:
https://www.chem.uci.edu/~dmitryf/manuals/Fundamentals/SLS%20Technologies%20GPC-SEC%20Explained.pdf
[Accessed 18 May 2020].

Malvern, 2020. *Analysis Model - Advice.* [Online]
Available at:
file:///C:/Program%20Files%20(x86)/Malvern%20Instruments/Zetasizer%20Software/Help/Default.htm?Highlight=algorithm#Advice/Result_calculation_-_Advice.htm?Highlight=algorithm
[Accessed 19 May 2020].

Mattison, K. & Nobbmann, U., 2011. *Evening Short Course (SC4): Dynamic Light Scattering Theory, Do's & Don'ts and Data Interpretation.* 4 ed. s.l.:Cambridge Healthtech Institute.

Maverakis, E. et al., 2014. Glycans in the immune system and The Altered Glycan Theory of Autoimmunity: A critical review.. *Journal of Autoimmunity,* Volume 57, pp. 1-13.

Nobbmann, U., 2017. *Aggregation Temperature (Tagg) - What is it, and How can we Calculate it?.* [Online]
Available at: https://www.materials-talks.com/blog/2017/11/16/aggregation-temperature-tagg-what-is-it-and-how-can-we-calculate-it/
[Accessed 18 May 2020].

Pronalyse, 2020. *Circular Dichroism Spectroscopy (Far UV).* [Online]
Available at: https://www.creative-proteomics.com/pronalyse/circular-dichroism-spectroscopy-far-uv.html
[Accessed 23 May 2020].

Raznikov, V. I., Treuheit, M. J. & Becker, G. W., 2015. Accelerated Formulation Development of Monoclonal Antibodies (mAbs) and mAb-Based Modalities: Review of Methods and Tools.. *Journal of Biomolecular Screening,* 20(4), pp. 486-483.

Schiel, J. et al., n.d. *NISTmAb Common Technical Document Case Study.* [Online]
Available at:
https://cdn.ymaws.com/www.casss.org/resource/resmgr/hos/HOS_2017_Workshop_Handout.pdf
[Accessed 22 May 2020].

Temel, D. B., Landsman, P. & Brader, M. L., 2016. Orthogonal Methods for Characterizing the Unfolding of Therapeutic Monoclonal Antibodies: Differential SCanning Calorimetry, Isothermal Chemical Denaturation, and Intrinsic Fluorescence with Concomitant Static Light Scattering. *Elviser Inc. ,* Volume 567, pp. 359-389.

Appendix

Method development

CD

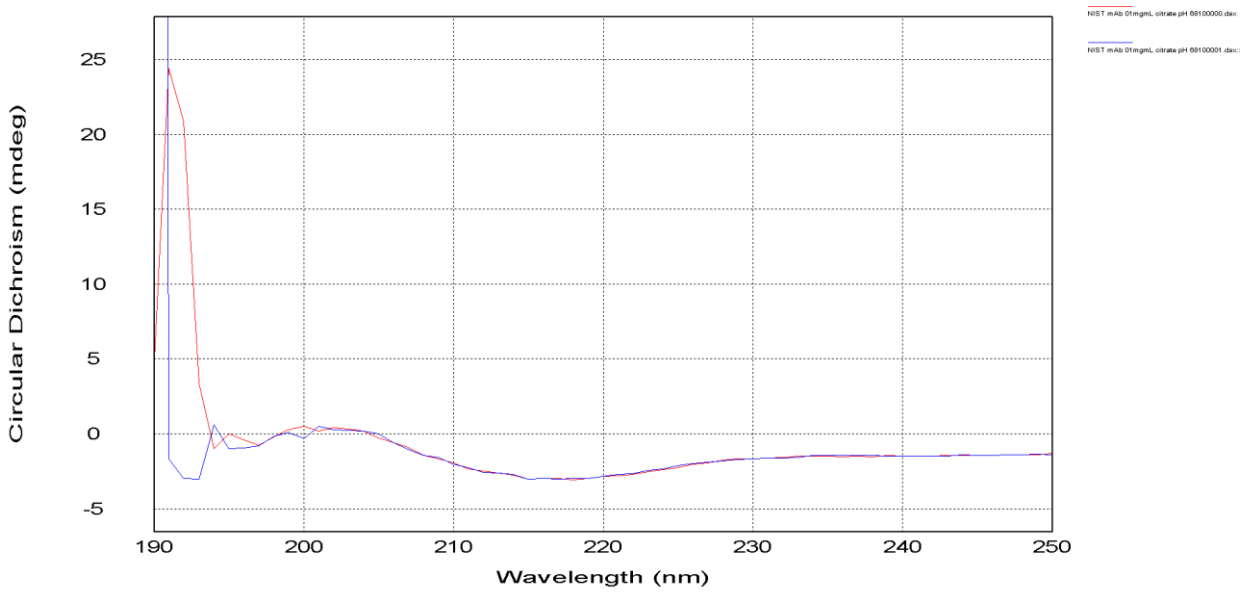

A1. The full far-UV scan of 0.1mg/mL NIST mAb in 25mM citrate buffer pH 6.81 scanned twice in a 0.5mm cuvette, using 1s per point between 190-250nm.

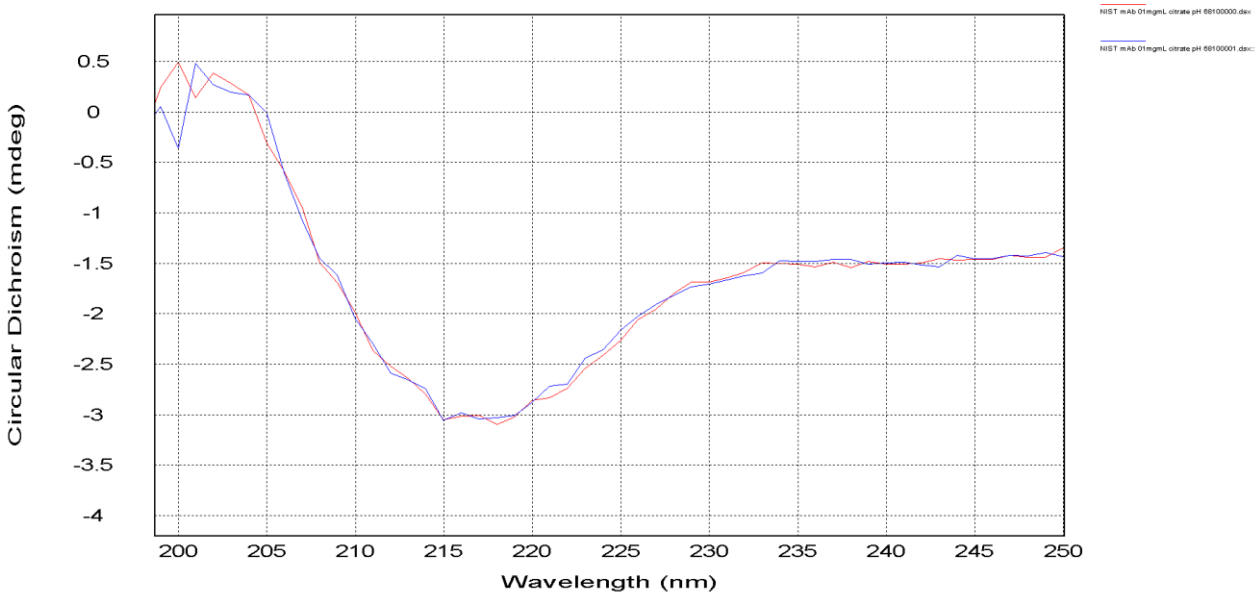

A2. The zoomed in far-UV scan of 0.1mg/mL NIST mAb in 25mM citrate buffer pH 6.81 scanned twice in a 0.5mm cuvette, using 1s per point between 190-250nm.

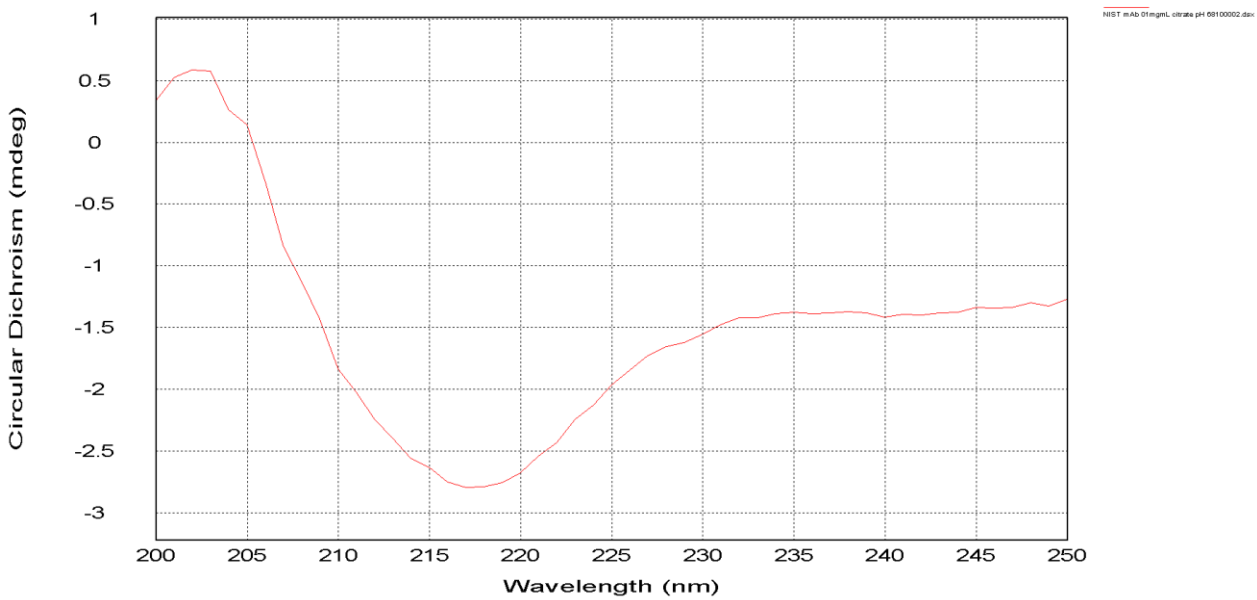

A3. A far-UV scan of 0.1mg/mL NIST mAb in 25mM citrate buffer pH 6.81 scanned in a 0.5mm cuvette, using 2s per point between 200-250nm.

DSC

Histidine buffer

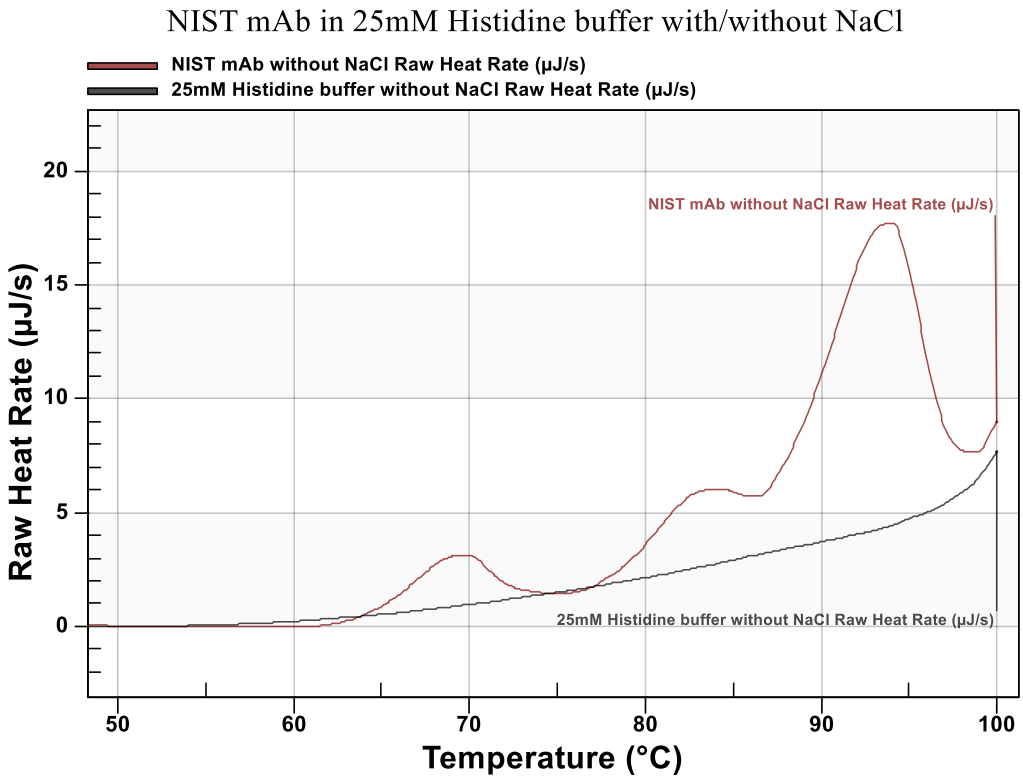

A4. The baseline (25mM Histidine buffer pH 6) and the 1.0mg/mL NIST mAb in a 25mM Histidine buffer pH 6 without 150mM NaCl.

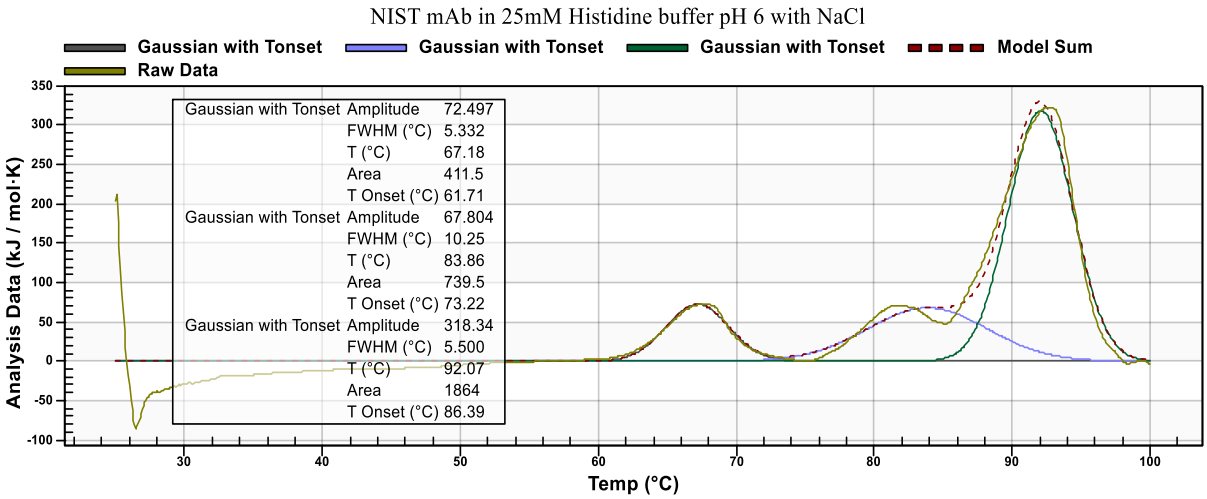

A5. 1.0mg/mL NIST mAb in 25mM Histidine buffer pH 6 with NaCl.

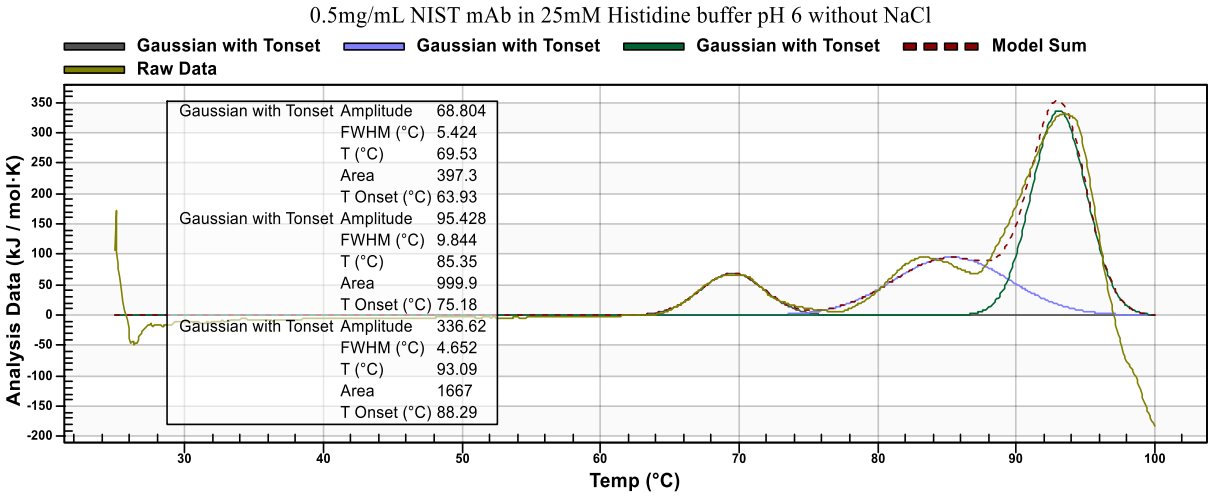

A6. 0.5mg/mL NIST mAb in 25mM Histidine buffer pH 6 without NaCl.

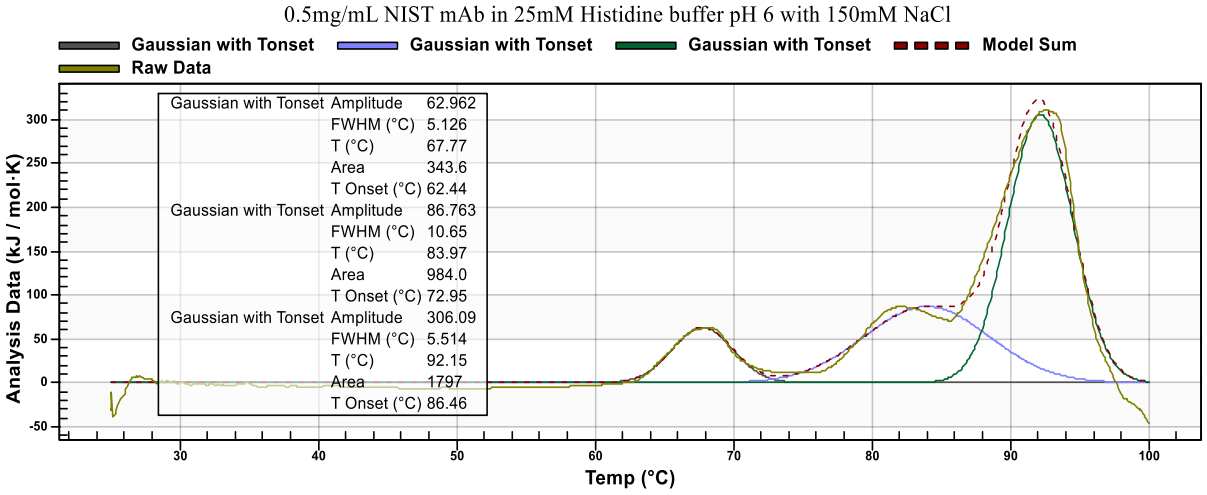

A7. 0.5mg/mL NIST mAb in 25mM Histidine buffer pH 6 with NaCl.

Citrate buffer

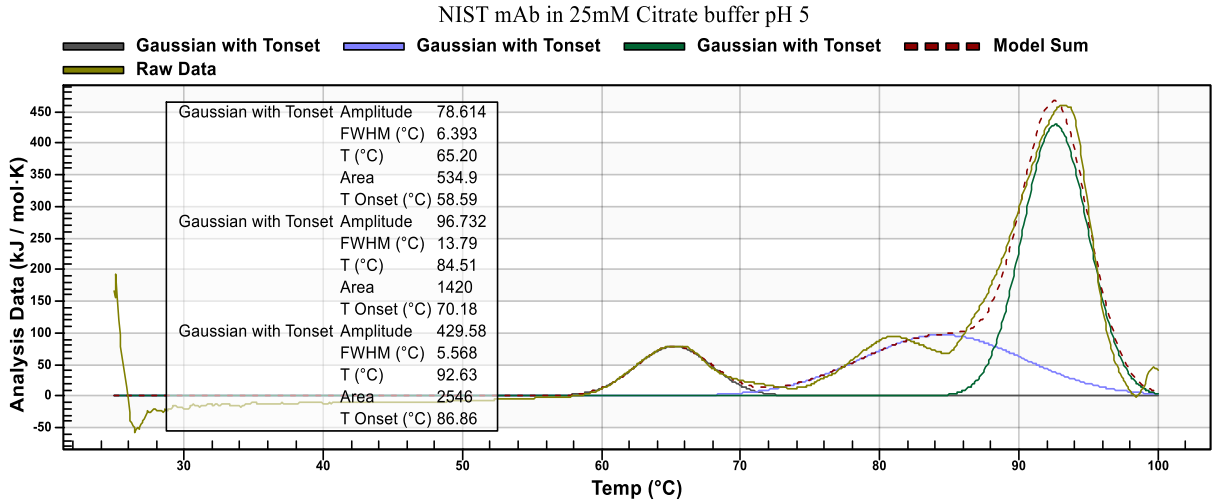

A8. 0.5mg/mL NIST mAb in 25mM Citrate buffer pH 5.

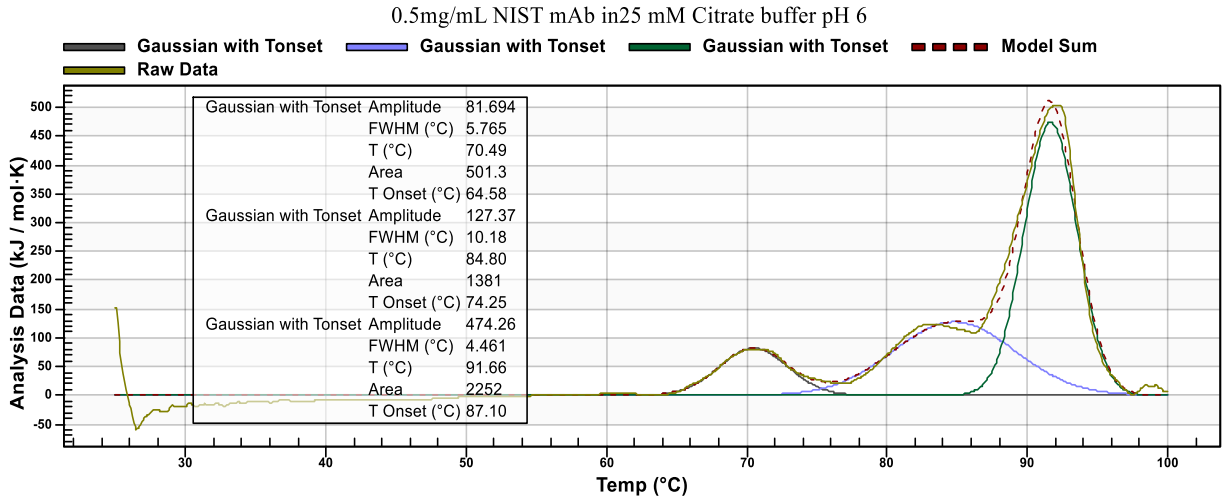

A9. 0.5mg/mL NIST mAb in 25mM Citrate buffer pH 6.

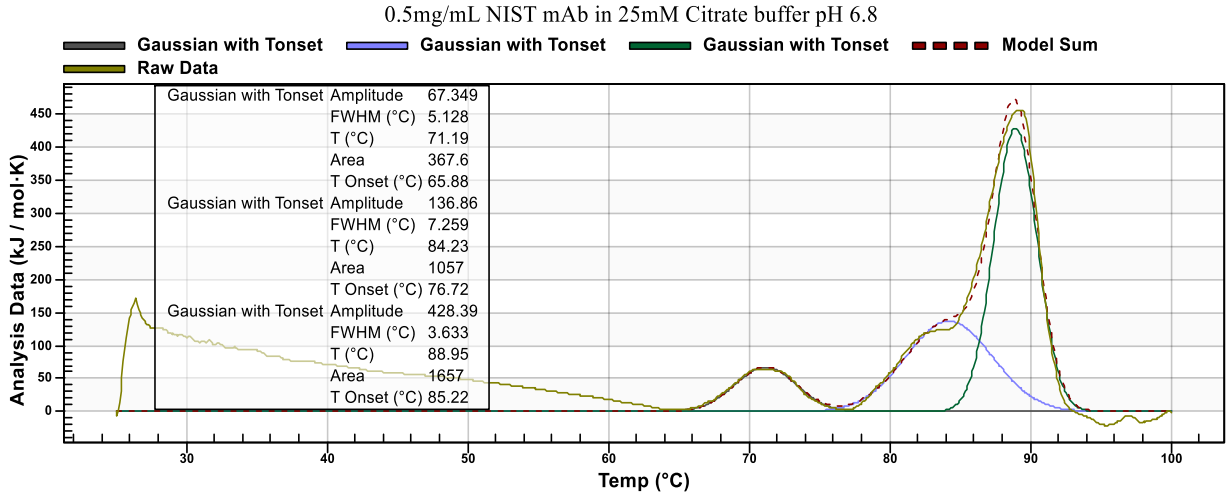

A10. 0.5mg/mL NIST mAb in 25mM Citrate buffer pH 6.8.

DLS

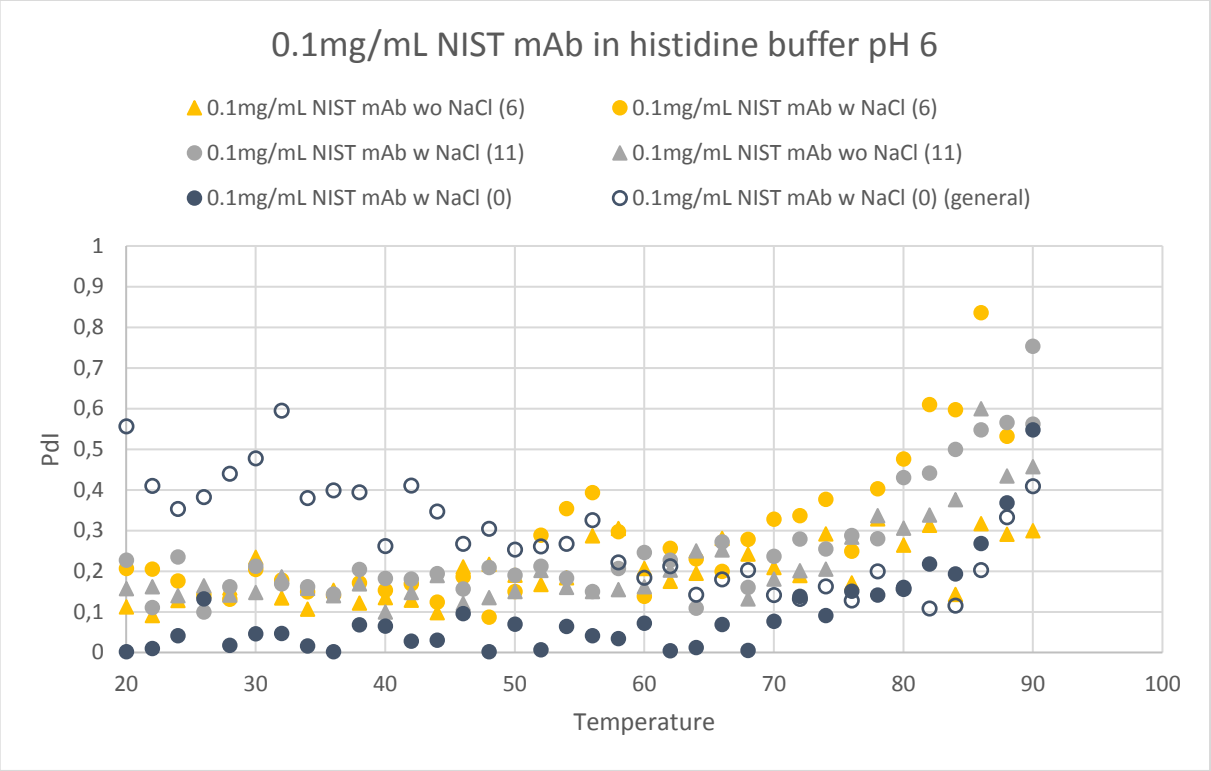

A11. The PdI vs temperature for the samples with a concentration of 0.1mg/mL NIST mAb in 25mM Histidine buffer pH 6 that were investigated using the Zetasizer.

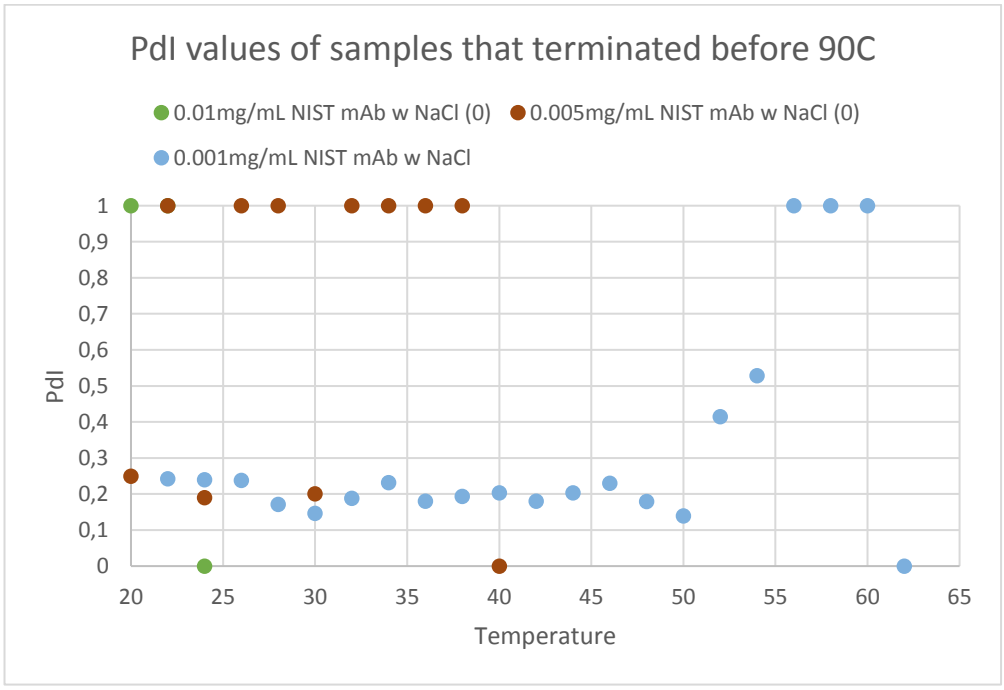

A12. The PdI-values of three samples that were terminated before 90°C by the Zetasizer software.

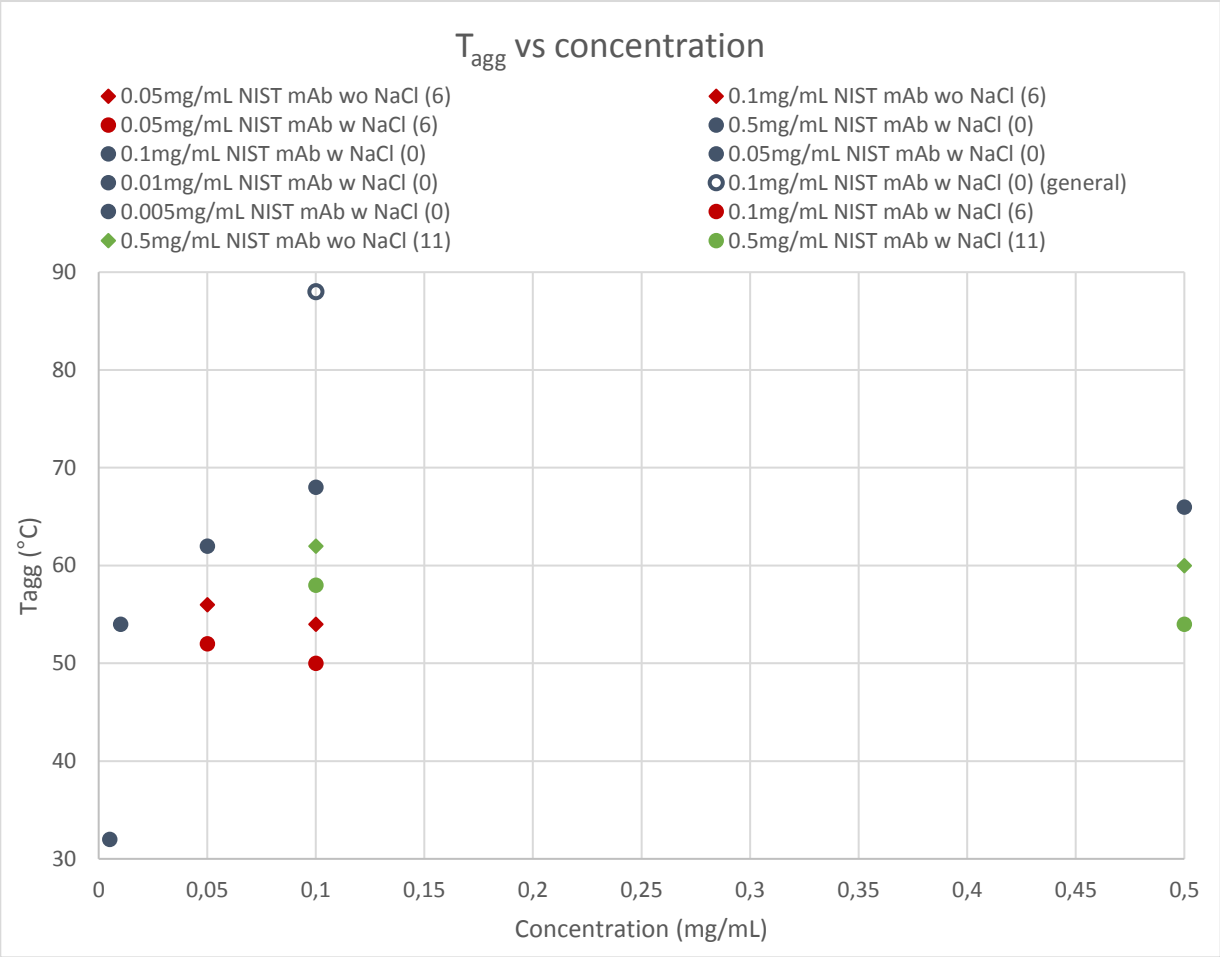

A13. The T_{agg} for the samples that were analyzed using the Zetasizer containing NIST mAb in 25mM Histidine buffer pH 6, in the concentration range from 0.005-0.5mg/mL, plotted against the concentration for the samples

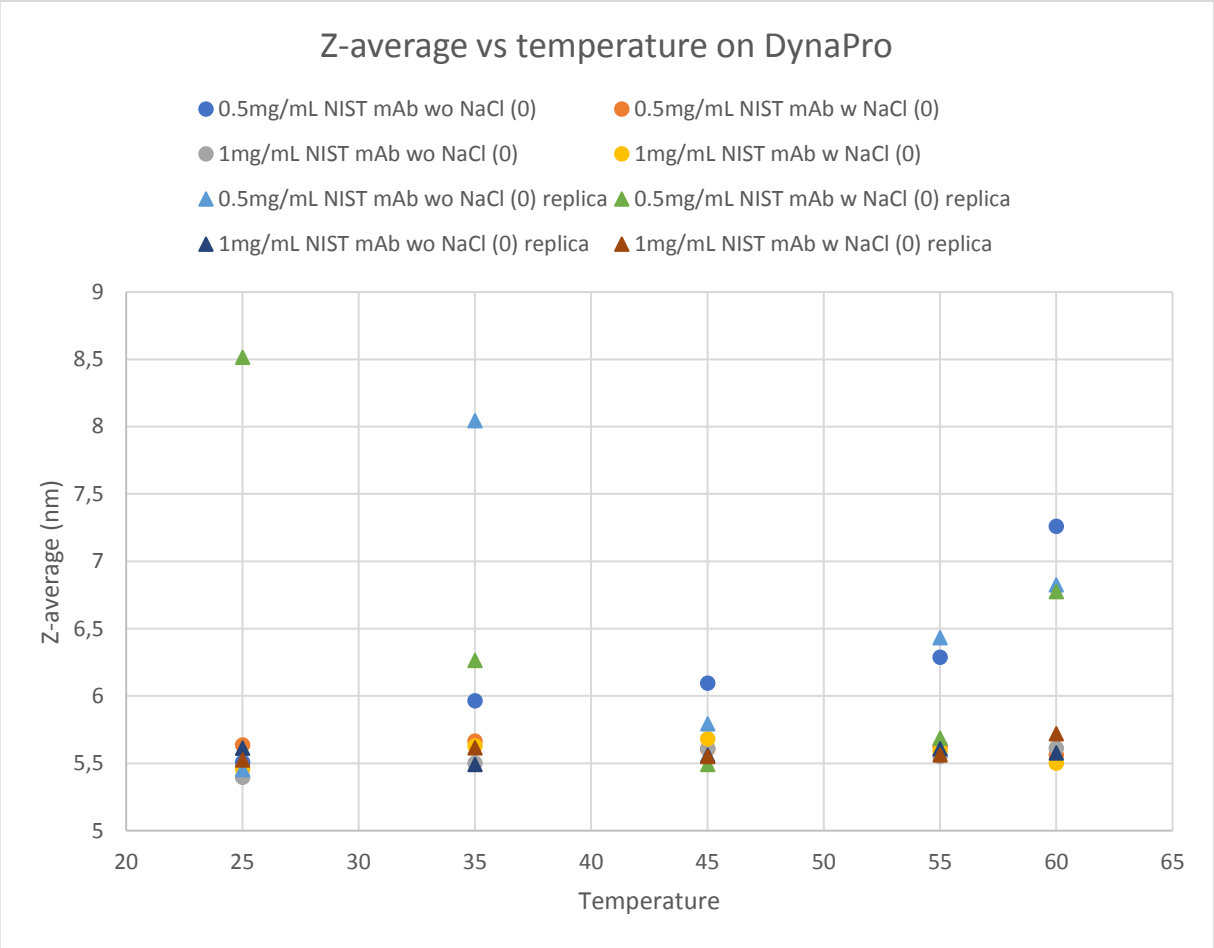

A14. The calculated Z-average plotted against the temperatures that were investigated on the DynaPro.

A15. Table over the complete chronological run order on the Zetasizer including each sample's storage time before the sample measurement, the measurement's end temperature and their estimated T_{agg}.

	Name of sample	Storage time (days)	T_{agg} (°C)	End temperature (°C)	Sample number
Histidine buffer	0.05mg/mL NIST mAb wo NaCl	6	56	90	1
	0.05mg/mL NIST mAb w NaCl	6	52	90	2
	0.1mg/mL NIST mAb wo NaCl	6	54	90	3
	0.1mg/mL NIST mAb w NaCl	6	50	90	4
	0.5mg/mL NIST mAb wo NaCl	11	60	90	5
	0.5mg/mL NIST mAb w NaCl	11	54	90	6
	1.0mg/mL NIST mAb wo NaCl	11	60	90	7
	1.0mg/mL NIST mAb w NaCl	11	60	90	8
	0.1mg/mL NIST mAb wo NaCl	11	62	90	9
	0.1mg/mL NIST mAb w NaCl	11	58	90	10
	0.1mg/mL NIST mAb w NaCl (general)	0	90	90	11
	0.1mg/mL NIST mAb w NaCl	0	70	90	12
	0.5mg/mL NIST mAb w NaCl	0	66	90	13
	0.05mg/mL NIST mAb w NaCl	0	62	90	14
	0.01mg/mL NIST mAb w NaCl	0	54	62	15
	0.005mg/mL NIST mAb w NaCl	0	24	40	16

	0.001mg/mL NIST mAb w NaCl	0	-	24	17
	0.1mg/mL NIST mAb wo NaCl	0	-	20	18
	0.5mg/mL NIST mAb wo NaCl	0	-	20	19
	0.05mg/mL NIST mAb wo NaCl	0	-	22	20
	0.01mg/mL NIST mAb wo NaCl	0	-	26	21
	0.005mg/mL NIST mAb wo NaCl	0	-	24	22
	0.001mg/mL NIST mAb wo NaCl	0	-	26	23
	0.1mg/mL NIST mAb w NaCl	0	-	20	24
	0.1mg/mL NIST mAb wo NaCl before freezing	18	N/A	N/A	25
	0.1mg/mL NIST mAb w NaCl before freezing	18	N/A	N/A	26
	0.1mg/mL NIST mAb wo NaCl after freezing	18	N/A	N/A	27
	0.1mg/mL NIST mAb w NaCl after freezing	18	N/A	N/A	28
Citrate buffer	0.005mg/mL NIST mAb wo cooling	0	64	90	29
	0.01mg/mL NIST mAb wo cooling	0	64	90	30
	0.05mg/mL NIST mAb wo cooling	0	-	46	31
	0.5mg/mL NIST mAb wo cooling	0	-	20	32
	0.005mg/mL NIST mAb w cooling	1	64	74	33
	0.01mg/mL NIST mAb w cooling	1	-	26	34
	0.05mg/mL NIST mAb w cooling	1	-	20	35
	0.05mg/mL NIST mAb w cooling no 2	1	62	70	36
	0.1mg/mL NIST mAb w cooling	1	62	90	37
	0.5mg/mL NIST mAb w cooling	1	-	20	38
MQW	Multiple measurements on MQW	N/A	N/A	N/A	39

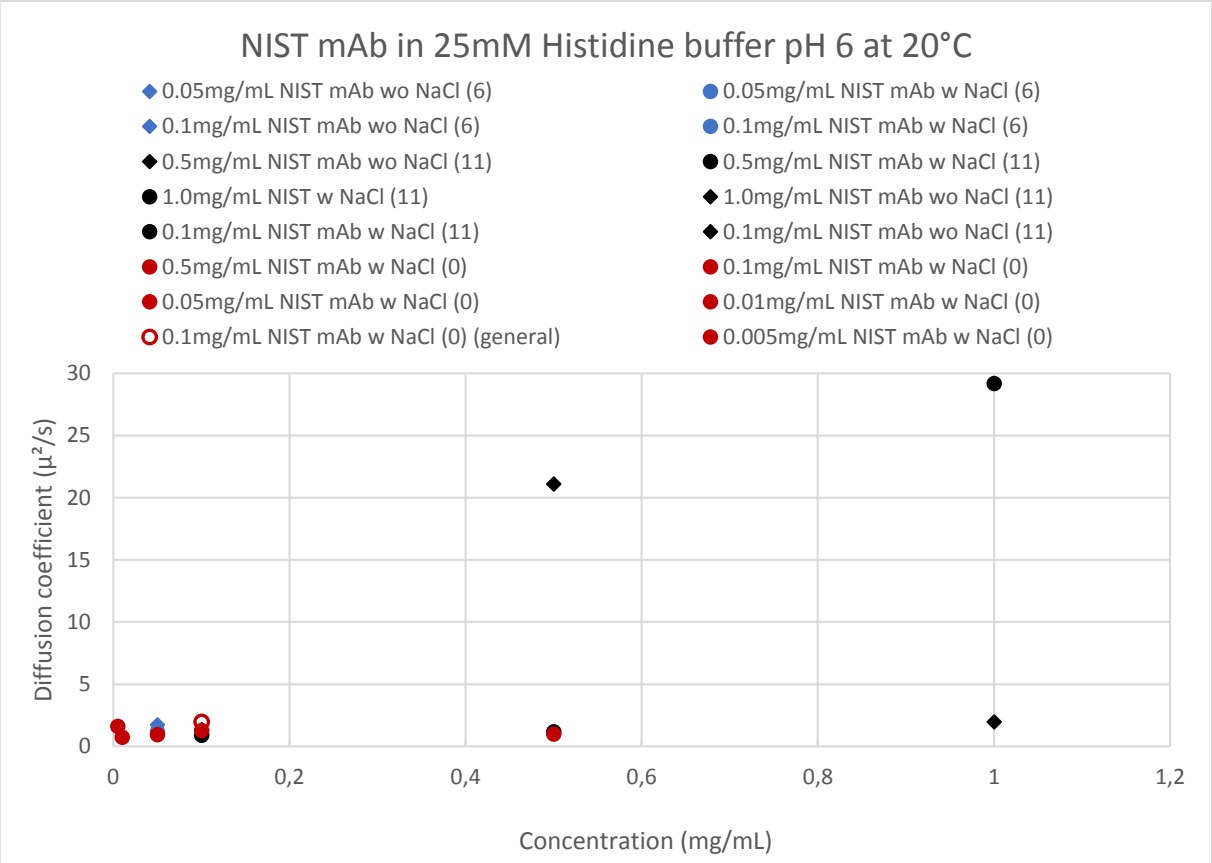

Appendix 16. The diffusion coefficient for NIST mAb in 25mM Histidine buffer pH 6 with and without 150mM NaCl plotted against the concentration.

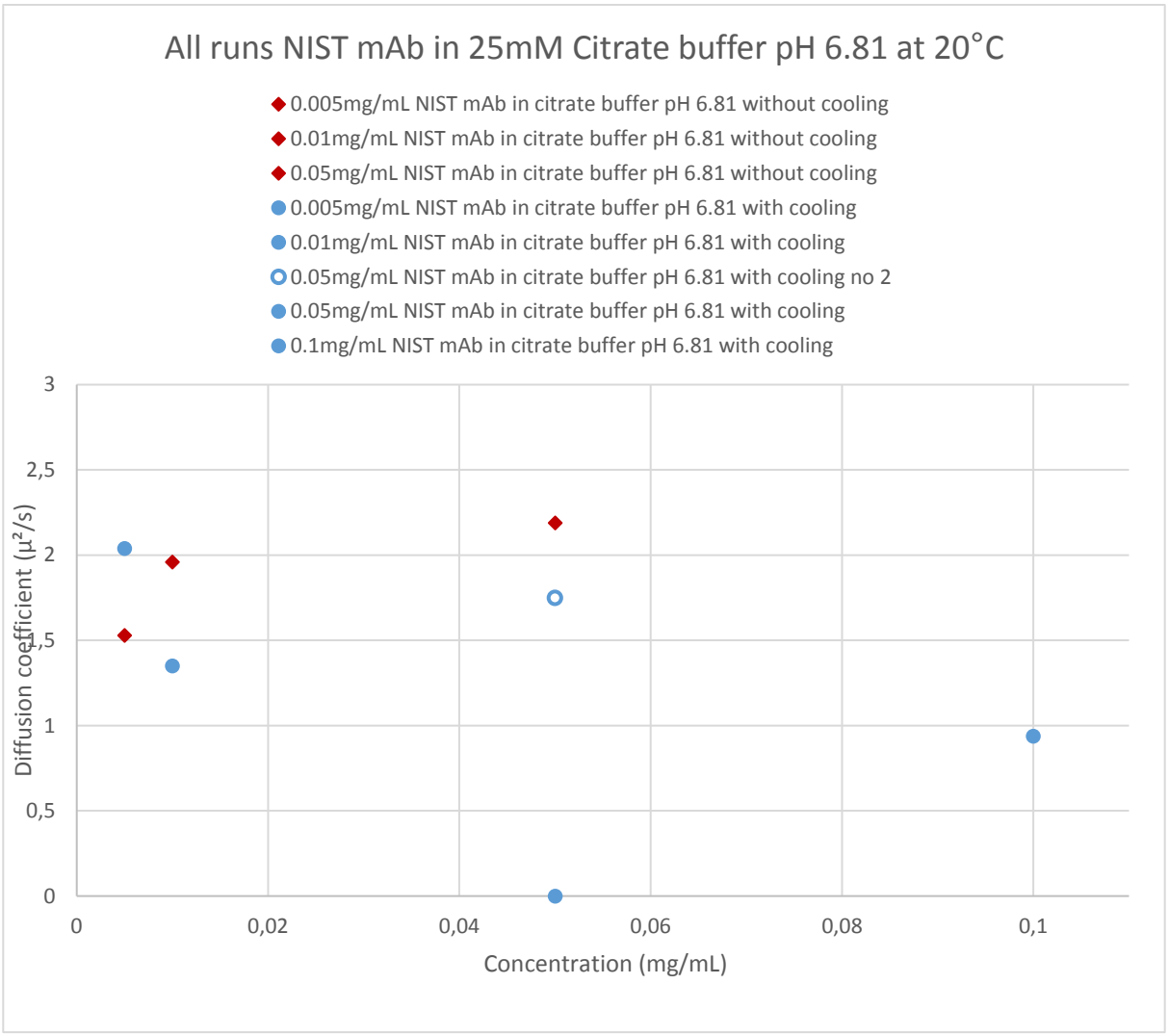

Appendix 17. The diffusion coefficient for NIST mAb in 25mM Citrate buffer pH 6.81 with and without cooling plotted against the concentration.

CD

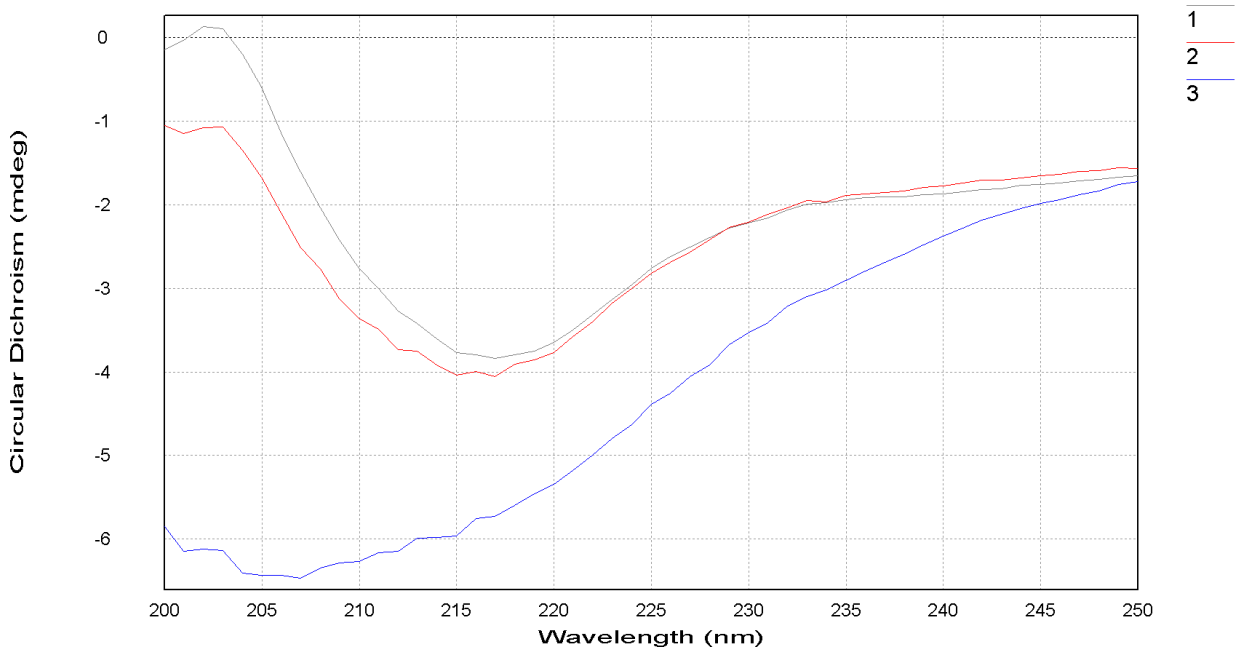

A18. The calculated far-UV spectra for the native state, first and second transition state of NIST mAb in 25mM Citrate buffer pH 5 during a temperature ramp between 20-90°C. The native state is called 1, the first transition state is 2, and the second transition state is 3.

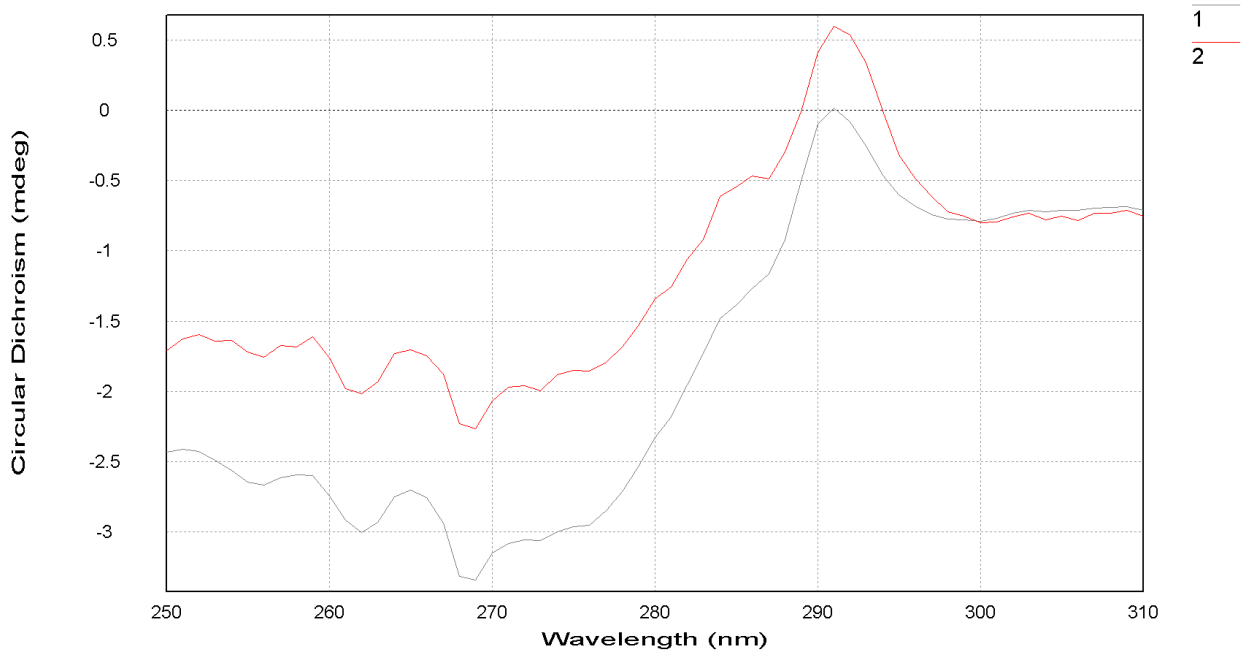

A19. The calculated near-UV spectra for the native state and the first transition state of NIST mAb in 25mM Citrate buffer pH 5 during a temperature ramp between 20-90°C. The native state is called 1 and the first transition state is 2.

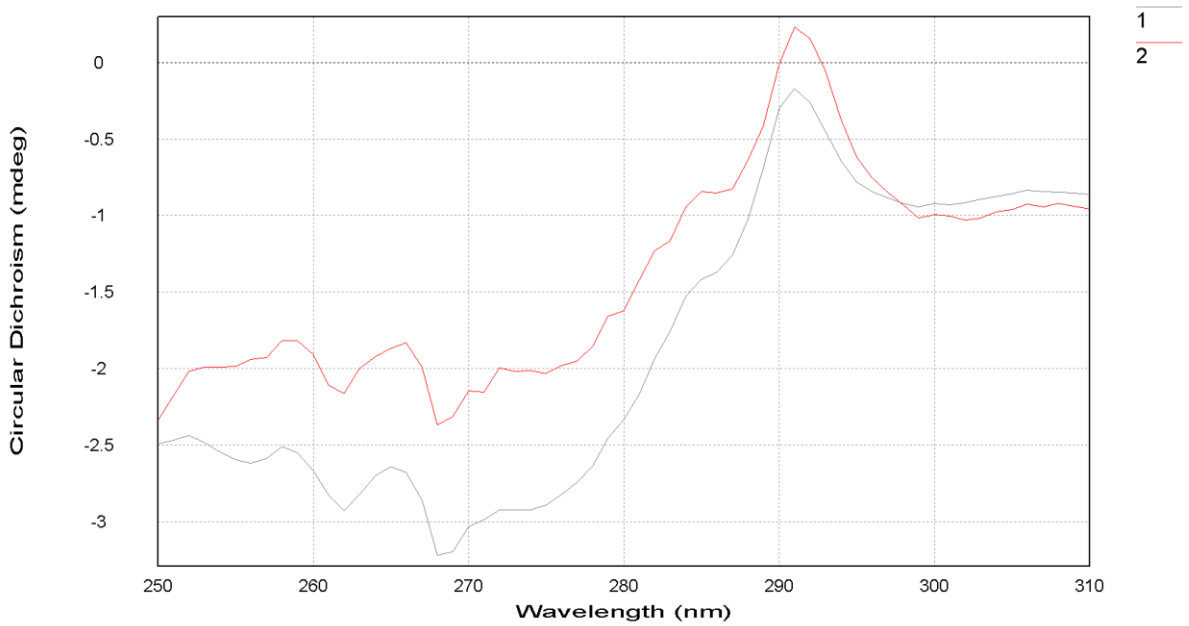

A20. The calculated near-UV spectra for the native state and the first transition state of NIST mAb in 25mM Citrate buffer pH 6 during a temperature ramp between 20-90°C. The native state is called 1 and the first transition state is 2.